Geologic Map and Structural Evolution of the Black Hills Creek Area in the Smash Minerals Whiskey Project, Yukon Territory

by

STACIE JONES

A THESIS SUBMITTED IN PARTIAL FULFILLMENT OF THE REQUIREMENTS FOR THE DEGREE OF

BACHELOR OF SCIENCE (HONOURS)

in

THE FACULTY OF SCIENCE

(Geological Science)

This thesis conforms to the required standard

……………………………………

Supervisor

THE UNIVERSITY OF BRITISH COLUMBIA

(Vancouver)

APRIL 2012

Abstract

This increase in activity in the Yukon-Tanana terrane from advances in the understanding of intrusion-related and orogenic gold mineralization, has led to the development of a joint academic-industry endeavour to further the magmatic, metallogenic and structural understanding of the area of interest. This project was developed and jointly- supported by Smash Minerals and the Yukon Gold Project, a joint MDRU-industry endeavour. Currently, the structural model developed by MacKenzie et al. (2006, 2008, and 2010) has helped elucidate the structural control on gold mineralization in the Golden Saddle deposit, Klondike District, and elsewhere in the western Yukon. Therefore, understanding the structural evolution of gold properties in the surrounding region is considered to be of considerable importance in locating new gold occurrences. The ultimate goal of this project was the construction of a geologic framework that respects all field observations. Supplementary analyses were used to define the structural evolution and timing and nature of mineralization of the Black Hills Creek area. The study area, approximately a 200m by 50m exposure of continuous bedrock, had been thoroughly exposed by previous placer operations along Black Hills Creek allowing for a detailed mapping study to be completed during the summer of 2011. Three main lithologic units were identified: a quartz-biotite schist, a quartzite and a felsic dyke. The entire map area had a pervasive foliation striking NW-SE and variably dipped to the SW. The felsic dyke commonly cuts this pervasive foliation at a low angle suggesting a later emplacement. U-Pb dating of monazites and zircons, using ID-TIMS and CA-TIMS methods, was done to establish ages of peak metamorphism and the timing of the felsic intrusion furthermore, Pb-isotopic analysis of sulphides were completed in an effort to correlate the timing and nature of mineralization to know mineralization in the surrounding areas. The study concluded that although all five phases of deformation anticipated from the model by MacKenzie *et al.* (2006, 2008 and 2010) are not present within the Black Hills Creek study area the structural evolution correlates with the regional development. With a peak metamorphic age of 260 m.y ago correlating to the Klondike orogeny and felsic dykes resembling both physically and chemically the Permian intrusives of the area it can be said that the Black Hills Creek area has a at least two events (D_2 and plutonic intrusions) that parallel the region model defined by MacKenzie *et al.*, (2006, 2008 and 2010).

Table of Contents

Chapter 4

Chapter 5

List of Figures

List of Tables

List of Plates

Acknowledgements

This project was developed and supported jointly by Smash Minerals and the Yukon Gold Project, a joint-MDRU-industry endeavour. Firstly, I would like to thank my supervisor Dr. Jim Mortensen for taking me on and introducing me to the Yukon Gold Project. Thank you for always giving me time, even when you were half way around the world. Thank you to Dr. Craig Hart, Dr. Murray Allan and the Yukon Gold Project team for welcoming me and guiding me throughout the duration of this project. I would also like to thank the encouraging geological team of Smash Minerals Corp; Adrian Fleming, Chris Siron, Chris Pennimpede and Rob Mackie, of Revelation Geosciences, for giving me time, resources and motivation to accomplish my field work. Lastly, I am indebted to Doug Mackenzie and Dave Craw for being invaluable sources of information, enthusiasm and inspiration.

Chapter 1

1.1 Introduction

Interest in the Yukon-Tanana terrane has increased over the past 25 years as advances in the understanding of intrusion-related and orogenic gold mineralization and high gold prices has permitted previously non-economic deposits to become feasible (Mortensen and Hart, 2010). Recent economic discoveries such as the Golden Saddle deposit in Underworld's White Gold property in 2008 has drawn attention and brought multi-million dollar exploration projects to the west-central Yukon (Mortensen and Hart, 2010). The exploration industry has responded by increasing Yukon quartz claims staking from 118 in 2005 to over 10,000 in 2007, with an additional 23,660 quartz claims staked between April 2009 and March 2010 (Global Business Reports, 2011). This increase in activity has led to the development of a joint academic-industry endeavour to further the magmatic, metallogenic and structural understanding of the area of interest. The Mineral Deposit Research Unit (MDRU) at the University of British Columbia has teamed up with twelve exploration companies (list provided in Appendix 1), forming the Yukon Gold Project, to facilitate more successful mineral exploration methods by conducting detailed studies on various mineral deposits and occurrences within the project area (Fig. 1).

Regional mapping and geochronological studies in the western Yukon have produced an overall understanding of the bedrock geology and the tectonic evolution of the region. Likewise, a structural model has been developed for the western Yukon although it has been pieced together from detailed studies of specific areas within a large territory of limited exposure.

Currently, the structural model developed by MacKenzie *et al.* (2006, 2008, and 2010) has helped elucidate the structural control on gold mineralization in the Golden Saddle deposit, Klondike District, and elsewhere in the western Yukon. Therefore, understanding the structural evolution of gold properties in the surrounding region is considered to be of considerable importance in locating new gold occurrences. Smash Minerals Corp., a junior gold exploration company carrying out gold exploration in the western Yukon, has a large property to the west of Kinross' White Gold property (Fig. 2). Although Smash Minerals is not part of the consortium of companies supporting the Yukon Gold Project, it was agreed that the research to be undertaken in this thesis would be beneficial for Smash Minerals on a property scale but would also generate site-specific information that would be of considerable value to the Yukon Gold Project

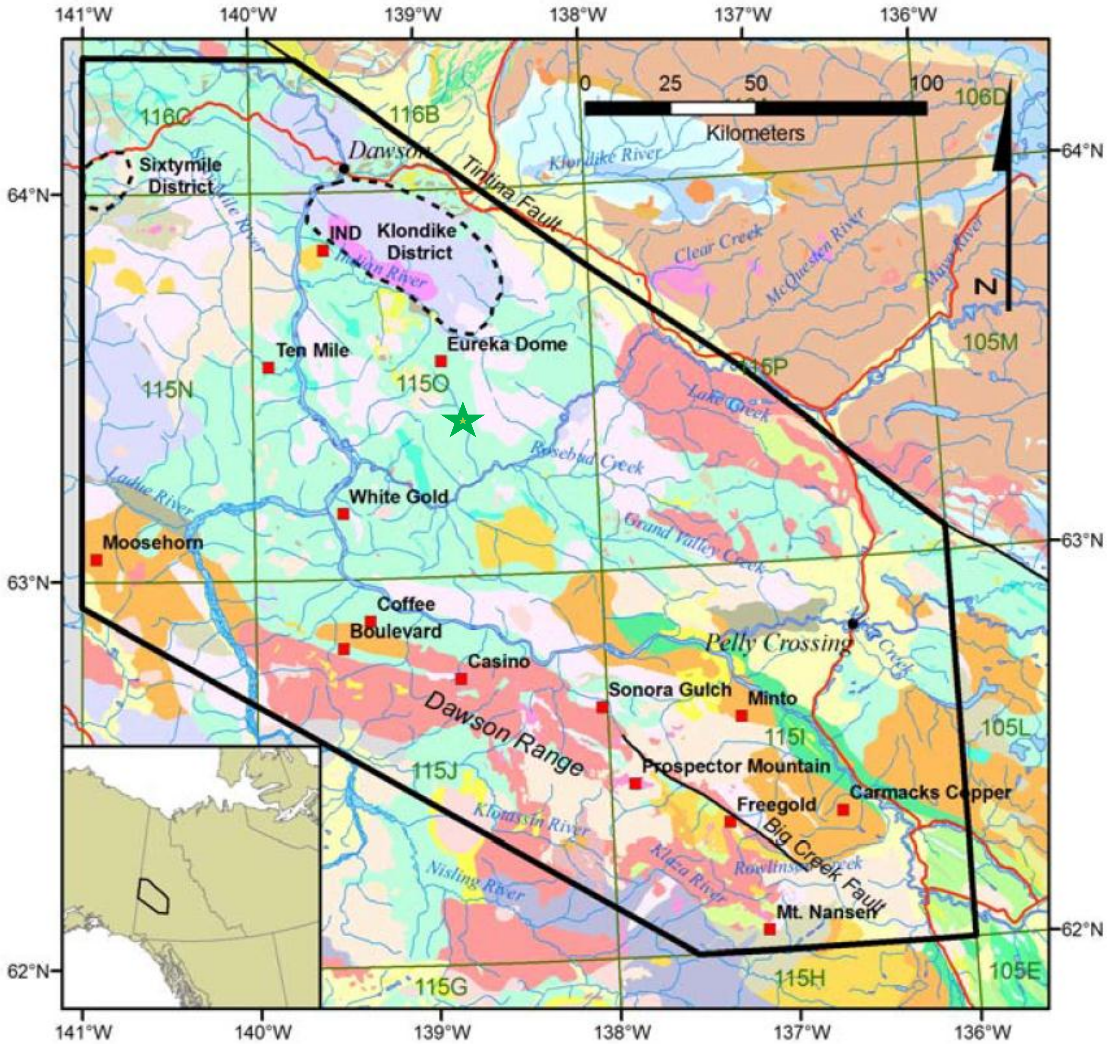

Figure 1: Regional geology of the Yukon Gold Project Study area between the Denali Fault to the southwest and the Tintina fault to the northeast. The Yukon Gold Project area is defined by the thick black polygon. The study area for this project is shown by green star.

The study area for this thesis is an approximately 200m by 50m exposure of continuous bedrock, which has been thoroughly exposed by previous placer mining operations along Black Hills Creek (Fig. 2). This exposure provided a unique opportunity, in a region of little to no outcrop, to document and map geologic features in the absence of cover. The purpose of this study was ***to improve the understanding of the structural evolution of the Black Hills Creek area and surrounding Smash Minerals property claims, with the intent of refining and testing***

the regional applicability of the structural framework developed for gold mineralization in the Klondike and White Gold areas as defined by MacKenzie et al. (2008 and 2010)

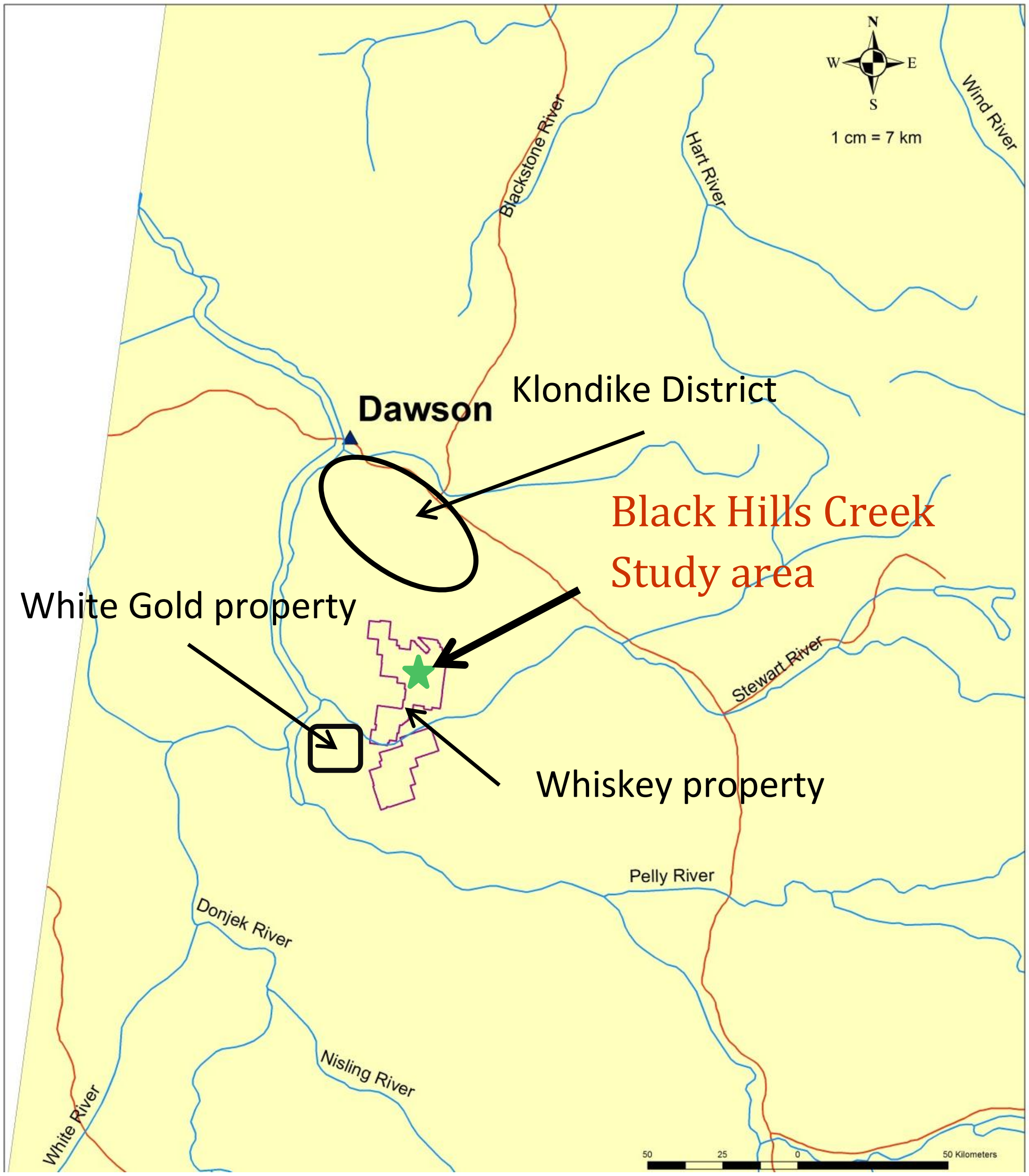

Figure 2: Map of western Yukon showing the location of the Smash Minerals' Whiskey property in purple and the White Gold and Klondike districts in black. The study area, along Black Hills Creek is denoted by the green star Scale: 1:7 00 000.

1.2 Previous Work

The project area lies between the well explored and geologically complex Klondike gold field to the north and the Stewart River area to the south. This part of western Yukon was first mapped on a regional scale by Bostock (1942), and subsequently by Mortensen (1996), Ryan and Gordey (2001, 2004), and Gordey and Ryan (2005). Detailed geological and structural studies were carried out in the Klondike District by Mortensen (1990) and MacKenzie et al. (2008), and in the White Gold area by MacKenzie et al. (2010). In addition a large amount of regional and property scale structural mapping has been carried out by researchers working with the Yukon Gold Project (M. Allan, J.K. Mortensen, L. Bailey, G. Mackenzie, and others, unpublished mapping). The understanding of the temporal and structural evolution of the western Yukon is still not fully resolved.

Chapter 2

2.1 Property Geology

The project area lies in what is known as the Stewart River area in the northern Cordillera in the western Yukon, along the western margin of the North American craton (Fig. 2 and 3). The Whiskey property of Smash Minerals extends north along Black Hills Creek, with a second claim block extending on the south side of the Stewart River. The study area lies south of the historic Klondike goldfield and northeast of the newly discovered White Gold district. This region is underlain by greenschist to lower amphibolite facies basement schist and gneiss of the Yukon-Tanana Terrane (Gordey and Ryan, 2005; Berman *et al.*, 2007). These rocks were metamorphosed and deformed in the Paleozoic through to Late Permian time, ending with the Klondike orogeny at the end of the Permian (Beranek and Mortensen, 2011; MacKenzie and Craw, 2012). The main underlying rock unit in this region consists of meta-siliciclasitc rocks (quartzite, quartz-muscovite schist and biotite schist) and meta-igneous rocks, mainly biotite-quartz-feldspar gneiss (Berman *et al.*, 2007; MacKenzie and Craw, 2012). Intermediate to mafic composition amphibolite bodies intrude and overlie the metaclastic rocks, which are in turn overlain by metapelites and carbonaceous quartzites of the Nasina assemblage (Gordey and Ryan, 2005; Berman *et al.*, 2007). These units were intruded by a variety of metaluminous metaplutonic rocks (Berman *et al.*, 2007). Episodic magmatic activity led to the emplacement of multiple generations of late syn- and post-tectonic

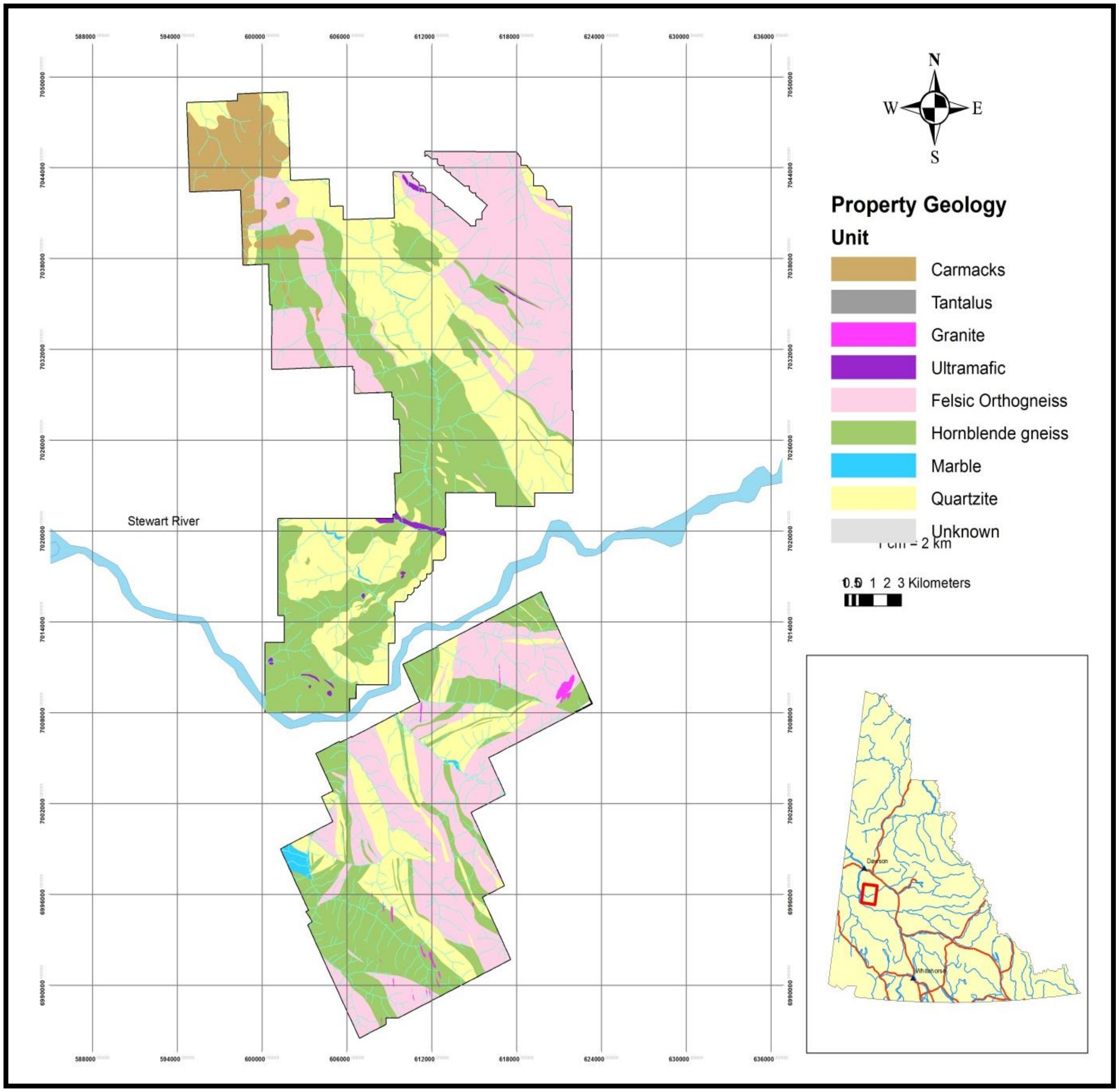

Figure 3: Geological map of the Whiskey property in the Stewart river area (geology by MacKenzie and Craw, 2012)

intrusions from latest Permian to early Tertiary time (Mortensen and Hart, 2010; Allan *et al.*, 2011). In the immediate region of the Smash Minerals claim blocks mafic and ultramafic units have been interpreted to represent slices of the Slide Mountain terrane that have been structurally imbricated with the metamorphosed basement rocks during Early Jurassic time (MacKenzie and Craw, 2012). Also, Late Cretaceous Carmacks Group mafic to intermediate volcanics occur in the northwest corner of the property (Fig. 3).

2.2 Tectonic Evolution

The North American Cordillera represents an active accretionary orogeny with a strike length of over 5000 km (Beranek and Mortensen, 2011). The Cordillera was assembled along the western margin of ancestral North America (Laurentia) starting in Precambrian time (Nelson and Colpron, 2007) and has been tectonically active since that time. It continues to be an important region of tectonic activity and formation of mineral deposits. Many years of intense study and mapping have led to the development of a tectonic model for the northern Cordillera centred on the concept of progressive accretion of tectonostratigraphic terranes. The northern Cordillera can be simplified into volcanic, plutonic and sedimentary units that have been metamorphosed by compressional forces during accretion (Berman *et al.*, 2007). These units are thought to represent accreted magmatic arcs, micro-continental blocks and fragments of closed ocean basins (Nelson and Colpron, 2007). The initial model of tectonostratigraphic terrane accretion was developed to explain how assemblages that show some affinity to the North American margin and others that have very different tectonic origins can become juxtaposed with one another after accretion to the continental margin (Nelson and Colpron, 2007).

Understanding the tectonic evolution of the northern Cordillera is essential for a better understanding of the distribution of mineral deposits in the region (Colpron *et al.*, 2006). It is important to note that tectonic evolution of the North American margin differed from the Yukon and British Columbia to the western United States; however, this paper will only focus on the evidence found in the Yukon.

The Yukon preserves the most complete geological record of magmatism, metamorphism and sedimentation associated with late Paleozoic and Mesozoic plate convergence and arc-continent collision along the length of the Cordilleran orogeny (Beranek and Mortensen, 2011). A simplified terrane map of the northern Cordillera by Nelson and Colpron (2007) subdivides this region into five distinct tectonic components. Starting from the easternmost boundary of the Cordillera, these include: 1) Ancestral North America (Laurentia); 2) Intermontane terranes; 3) Insular and Farewell terranes; 4) Artic Alaska; and 5) Mesozoic arc and accretionary terranes. The Intermontane terranes (which include the Yukon-Tanana terrane) refer to those terranes that show a pericratonic (continental) nature and an affinity to northwestern Laurentia, whereas the Insular and Farewell terranes are exotic and show no Laurentian linkages (Fig. 4)

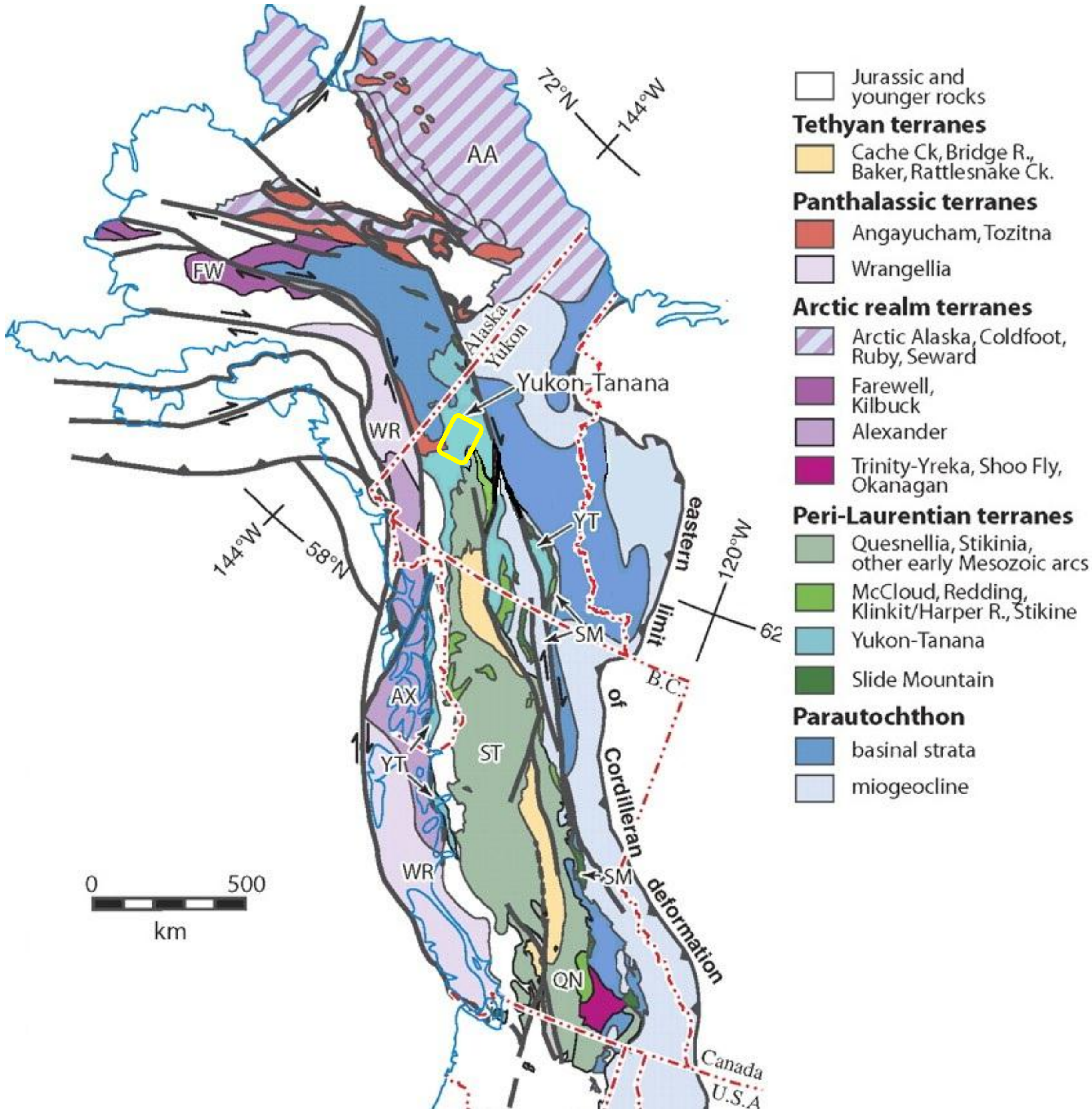

Figure 4: A simplified map of the lithotectonic terranes identified by Nelson and Colpron (2007), this figure is modified from Piercy and Ryan (2009). The yellow rectangle denotes the approximate location of the Whiskey Property.

In Neoproterozic time Laurentia broke apart from the Siberian Platform, dividing the supercontinent Rodinia and creating a west-facing passive margin that experienced little tectonic activity until mid-Paleozoic time (Nelson and Colpron, 2007). After an interval of approximately 400 m.y., in Late Devonian time Laurentia saw an increase in arc magmatism. During Late Devonian and Early Mississippian time east-dipping subduction beneath the Laurentian margin initiated the formation of a continental magmatic arc. As subduction continued extension in the back-arc region separated the magmatic arc (basement to the Yukon-Tanana terrane) from the Laurentian margin and formed the back-arc basin known as the Slide Mountain Ocean (Nelson and Colpron, 2007). Subsequent subduction polarity reversal and closure of the Slide Mountain Ocean by west-dipping subduction in Late Permian time led to the formation of the Late Permian Klondike arc. This shift ultimately led to strong deformation and metamorphism of the arc during the final closure of the Slide Mountain Ocean, thereby accreting the Yukon-Tanana arc onto the northwestern margin of Laurentia (Beranek and Mortensen, 2011). The project area lies within the accreted Yukon-Tanana terrane.

The Yukon Tanana terrane in western Yukon is a composite of four major lithotectonic assemblages (Colpron *et al.*, 2006). The pre-Late Devonian Snowcap assemblage represents a continental margin assemblage of metasedimentary and metavolcanic rocks. The isotopic compositions of the metasedimentary units suggest a Laurentian affinity (Piercey and Ryan, 2009). The Snowcap assemblage is overlain by the Finlayson assemblage, a mid-Paleozoic arc and back-arc assemblage, and subsequently by the Klinkit and Klondike assemblages which formed as younger superimposed arc assemblages (Beranek and Mortensen, 2011).

The Klondike arc is the youngest assemblage in the Yukon-Tanana terrane and formed in Middle to mainly Late Permian time (Beranek and Mortensen, 2011). It is interpreted to document the closure of the Slide Mountain ocean following subduction polarity reversal (Nelson and Colpron, 2007; Beranek and Mortensen, 2011). The maximum width of the Slide Mountain Ocean had not been determined because the duration of magmatism and the timing of emplacement of the Klondike arc was uncertain. However a recent study by Beranek and Mortensen (2011) demonstrated that accretion of the Yukon-Tanana terrane occurred in latest Permian time.

Following the arc accretion, metamorphism and crustal thickening continued, leading to several distinct magmatic pulses from Late Triassic to Late Cretaceous time (Mortensen and Hart, 2010). The Late Triassic and Early Jurassic (218-185 Ma) intrusions are metaluminous, strongly oxidized and show continental arc geochemical signatures (Mortensen and Hart, 2010). The Early Cretaceous magmatic pulse (~112-99 Ma) spans an area greater than 400 km from the Denali Fault far to the east onto the North American continent (Mortensen and Hart, 2010). This pulse comprises calc-alkaline intrusions of continental affinity to the southwest but youngs to the northeast and shifts to a more reduced composition indicative of a retro-arc setting (Mortensen and Hart, 2010). The last magmatic phase occurred in the Late Cretaceous as calc-alkaline intrusions in the Dawson Range (~72-78 Ma) and a more extensive series of intrusive and volcanic rocks (Carmacks Group from 72-69 Ma; Mortensen and Hart, 2010). Subsequently in Eocene time the Yukon-Tanana terrane was displaced by 430 km of dextral slip along the Tintina Fault to its current position (Nelson and Colpron, 2007).

2.3 Structural Model of the Yukon-Tanana terrane in western Yukon

Detailed studies of the structural evolution of the Yukon-Tanana terrane have been carried out in the Klondike goldfield by MacKenzie *et al.* (2008) and in the White Gold area by MacKenzie *et al.* (2010). Subsequent regional structural work being done by the Yukon Gold Project and others in the Yukon-Tanana terrane suggest that the structural models that came out of the previous work also apply at least in a general way throughout a large region from eastern Alaska to western Yukon (Allan *et al.,* 2011).

Structural work in the Klondike and White Gold areas by MacKenzie *et al.* (2008 and 2010) recongnized five distinct deformation phases. The Klondike Schist in the Klondike District forms the upper part of a stacked pile of thrust panels which include the Nasina Assemblage and slices of greenstone and ultramafic rocks of the Slide Mountain terrane (MacKenzie *et al.,* 2006). The Klondike Schist is structurally more complex than the underlying units and displays structures that progressively evolve through the ductile-brittle transitions (MacKenzie *et al.,* 2006; Allan *et al.*, 2011).

In the Klondike Schist initial depositional layering (S_0) can no longer be recognized; however, a pervasive foliation represents a composite structural feature of early metamorphic foliation (S_1) that has been reactivated by ductile deformation (F_2) during peak metamorphism (MacKenzie *et al.,* 2006). The pervasive foliation (S_2), that was imposed sub-parallel to parallel to S_1, is defined by the alignment coarse grained metamorphic micas and now generally displays shallow dips over the entire area except where later deformation has caused steepening (MacKenzie *et al.,* 2006 and 2008). In addition, the development of the pervasive foliation also produced metamorphic segregations (mm to cm scale) that finely laminated the rocks, and simultaneously generated foliation parallel quartz veins (MacKenzie *et al.*, 2006).

F_1 and F_2 structures are not commonly observed in the Klondike schist; however, more prominent overprinting folds (F_3) present as minor structures found as part of larger scale recumbent folds (MacKenzie *et al.*, 2006). The F_3 folds formed a prominent crenulation cleavage (S_3) parallel to the F_3 fold axial surface which is emphasised by the lineation of the S_3 intersecting with the foliation (Figure 2; MacKenzie *et al.*, 2006). S_3 cleavage surfaces are

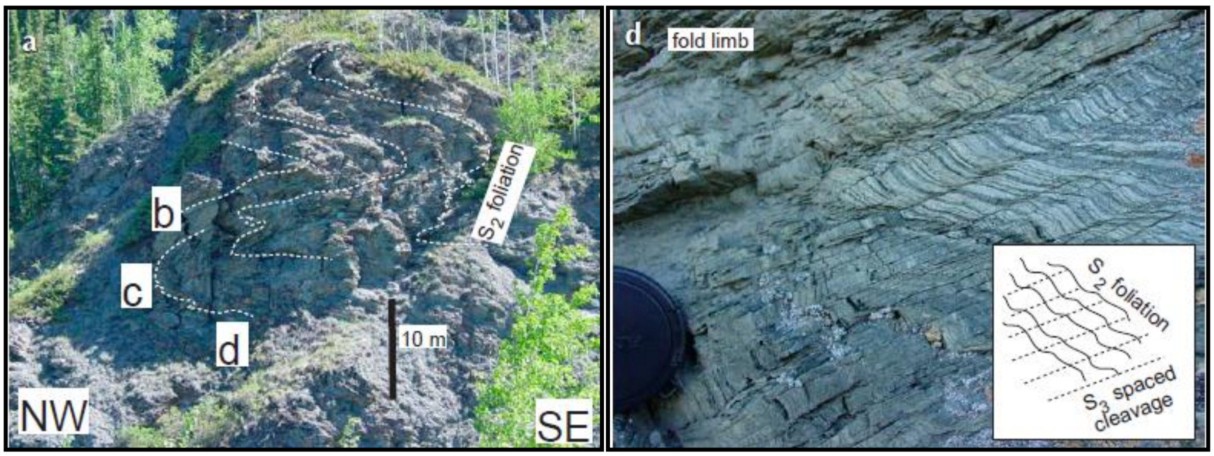

Figure 5: This figure shows the different structural features observed in the Klondike District (from MacKenzie *et al.* (2006). These photos show a set of recumbent F_3 fold in the Nasina Assemblage 2 km above the mouth of the Bonanza Creek. Photograph (a) shows the whole outcrop with S_2 foliation outlined by the white dashed lines. Photograph (d) shows the relative angular relationship of the S_2 foliation and the S_3 spaced cleavage

spaced (between 0.1 -10m apart) and are polished showing slickensides with minor recrystallization of chlorite (MacKenzie *et al.*, 2006).

The Klondike Schist is then cut by reverse faults and related kink folds (F_4) (MacKenzie *et al.*, 2006). The formation of the kink folds varies and some areas show no evidence of D_4 whatsoever. When present, the folds and faults deform F_3 structures and distort the pervasive foliations. The most distinct features are meter-scale fault gouge and scattered kink folds (MacKenzie *et al.*, 2006). This phase of deformation signifies the change from a ductile environment to a brittle-ductile regime.

Table 1. Comparison of structural evidence found in the Klondike District and White River area.

Regional Deformation Event	White River area Structures	Inferred age	Klondike District Structures
D_5	Normal faults (striking N and E) and meter scale felsic dykes	Middle Cretaceous-early Tertiary	Normal faults with felsic and mafic dyke and hydrothermal alteration
D_4	Rare upright kink folds, No veins	Jurassic	Upright kink folds of foliation, with some quartz veins in axial surface fractures.
Bimodal intrusions	Sills intruded into D_3 deformations zones	Late Triassic-early Jurassic	Absent
D_3	Folds, shears and chloritic foliation, especially associated with ultramafic horizons	Late Triassic –early Jurassic	Folds with spaced cleavage
D_2	Pervasive amphibolite facies foliation, rare isoclinal folds	Late Paleozoic	Pervasive greenschist facies isoclinal folds, fold axial surface foliation
D_1	Mostly overprinted by D_2 structures	Late Paleozoic	Folds of bedding

The fifth phase of deformation identified by MacKenzie *et al.* (2008) is recognized as normal faults during the Late Cretaceous and is associated with regional extension (Mortensen, 1996; MacKenzie *et al*., 2008). These normal fault typically have a N to NE and W to NW strike and cross cut all early structural featres (MacKenzie *et al.*, 2008). They also commly show evidence of hydrothermal activity, including local pyritizaton and silicification (MacKenzie *et al.* 2006). These structural generations distinct in the Klondike Schists do not necessarily corresponds to generation of structural events in other thrust slices (MacKenzie *et al.*, 2008).

The White River area to the west of the Whiskey property consists of similar Paleozoic schist and gneisses as in the Klondike District (MacKenzie *et al.*, 2010). Table 1 shows the comparison between deformation events and related structures in the Klondike District and the White River area.

The metamorphic grade in the Yukon-Tanana terrane in western Yukon varies from lower to middle greenschist facies in the Klondike District to lower amphibolite facies in the White River area. However the prevasive foliation (S_1+S_2) is still recognizable in the high grade rocks (MacKenzie *et al.*, 2010). D_1 and D_2 timing can be constrained by relationships between the Sulphur Creek orthogneiss, a felsic orthogneiss body contained in the Nasina Assemblage, and the Jim Creek pluton (Beranek and Mortensen, 2011). The Sulphur Creek orthogneiss and the felsic orthogneiss within the Nasina, found in the southwest area of the Klondike District, both contain D_1 and D_2 structures and give U-Pb zircon crystallization ages of 260Ma (Beranek and Mortensen, 2011). The Jim Creek pluton is massive, and displays neither D_1 nor D_2 structures and is dated at 252.5 Ma (Beranek and Mortensen, 2011). Therefore, deformation phases D_1 and D_2 must have concluded before emplacement of the 252.5 Ma intrusions. MacKenzie *et al.* (2006 and 2008) suggest that no mineralization occurred during these stages of deformation, although minor intrusion related Au and Bi mineralization has been recognized associated genetically with the Jim Creek pluton itself (Allan *et al*, 2011). D_3 is regionally associated with the regional scale thrust emplacement of structural slices of Slide Mountain terrane, whereas D_4 signifies the transition from ductile/brittle to brittle-ductile regimes (MacKenzie *et al.*, 2006, Allan *et al.*, 2011).

In the White River area five deformation events broadly similar to the phases identified in the Klondike District are still assumed to have taken place; however, evidence is not as apparent in this region as in the relatively well exposed and well studied Klondike Schist. For example, the third phase of deformation produced spaced cleavages in the Klondike District but in the White River area D_3 is associated with folds and foliation development with abundant chlorite (MacKenzie *et al.*, 2010). Furthermore, D_3 in the White River area commonly generated zones of weakness for intruding sills whereas in the Klondike Distict there are no such associated intrusions (Berman *et al.*, 2007; MacKenzie *et al.*, 2008). In addition, the fourth deformation phase observable in the Klondike District as kink folds and reverse faults is rarely seen in the

White River area. This phase of deformation, however, is thought to be associated with Au-bearing orogenic veins in the White River area, as in the Klondike (MacKenzie *et al.*, 2008 and 2010).

Chapter 3

3.1 Field Mapping Techniques

The study area, an approximately 200m by 50m exposure of continuous bedrock, had been thoroughly exposed by previous placer operations along Black Hills Creek. This exposure provided a unique opportunity, in a region of little to no outcrop, to document and map geologic features in the absence of cover. Mapping for the study began in early July of the 2011 field season with the creation of a detailed base map on which to record the geological data.

To begin, meter high posts and colourful flagging tape were used to construct a grid dividing the 200m X 50m study area into twenty-eight 25m X 15m zones. This grid was necessary to facilitate navigation while mapping. Since the accuracy of the Trimble GPS units available were on the order of meters (3m-7m) they could not be relied upon to map such a small area. The grid was fashioned to known specifications to enable pinpointing the location of each geologic feature in a defined zone.

Once the grid was finished, aerial photographs were taken at varying elevations from an AStar helicopter with the door removed. Once in the helicopter it quickly became apparent that the ability to observe the study area from an elevated vantage point would be beneficial and in the end necessary. The aerial photos were detailed enough to show key features such as the well-defined felsic dykes that can be seen trending NW-SE across the grid (Fig 7). The photos were also extremely valuable for attempting to discern what material had been previously displaced by the historic placer operations (Fig. 6). Next, the photos were georeferenced using the computer program Global Mapper. Using one GPS point taken in the north-east corner of the grid as a reference point the remaining UTM coordinates of the posts could be calculated. From these calculated UTM coordinates the photos were arranged in space and could be inputed into a mapping program such as ArcGIS.

Figure 7 shows the stitched mosaic of 5 photos taken from the helicopter. The yellow star represents the key post where the UTM coordinate was originally taken and the blue dots are the calculated locations of the map area boundaries. The mapping was done in three phases. The first phase involved documenting geologic features using two methods. One focused on locating features using a measuring tape and the calculated grid which was then recorded on sheets Mylar at a scale of 1:200. The other method involved a highly accurate and precise Trimble GPS unit that was on average accurate within 30cm. This instrument was not available until the majority of the mapping had been completed by hand; however, it greatly improved the speed of recording geological data during the final stages of mapping.

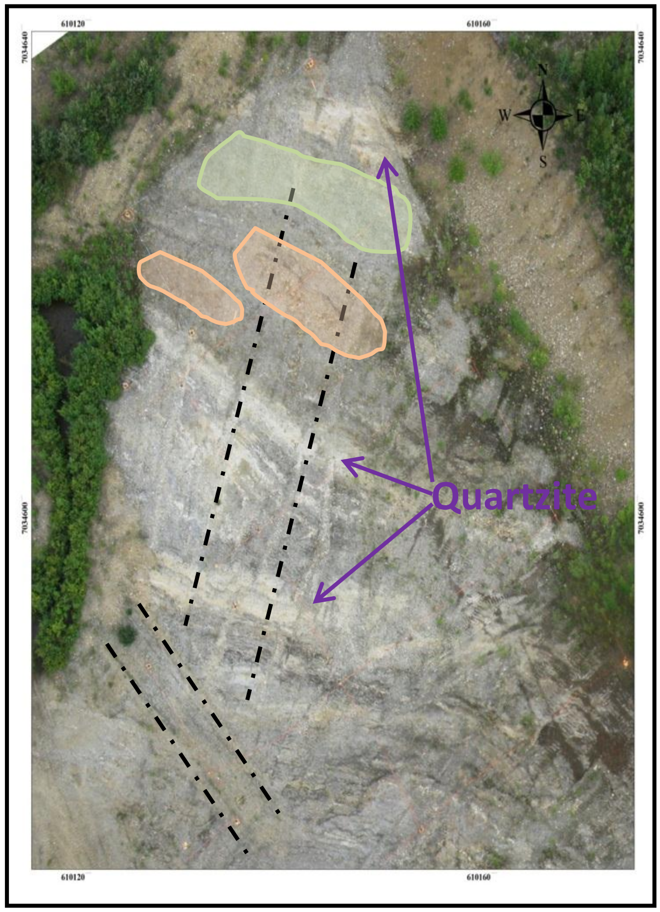

Figure 6: Showing the northern section of the detailed mapping area. The black hash lines indicate the line of disturbance from the previous placer workings. The green polygon identifies an area of consistent well foliated fine grained schist whereas the orange polygons denote zone of competent, gossanous schist with cm scale quartz segregations.

The second phase of the mapping concentrated on structural features. A total of 84 structural measurements of foliations, fractures, and fold axis orientations were taken. The last phase included sampling all lithologies and mineralized zones for specific geochemical and geochronological analysis. There were 38 samples collected in total. The locations of all structural measurements and all samples were recorded using the Trimble GeoXH handheld device. All of this GPS data was exported from the device and then imported into ArcMAP 10 and made into point layer files. The final map product was a combination of the manual Mylar mapping and the Trimble handheld mapping (Plate 1). The Mylar sheets were digitized and integrated into the Trimble`s exported data layers.

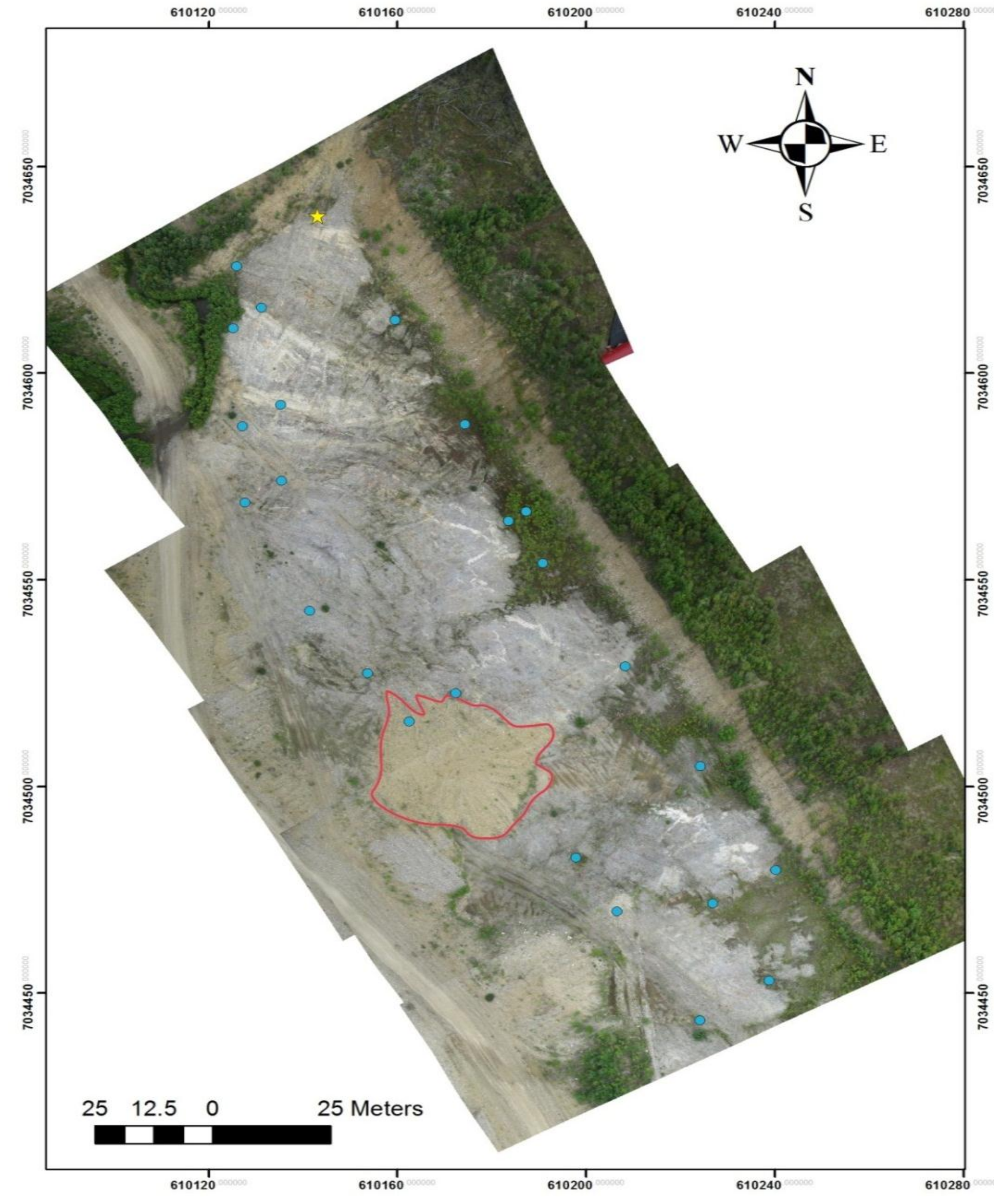

Figure 7: This figure shows a mosaic of five georeferenced aerial photographs of the study area taken from an Astar helicopter. The yellow star represents the key post where the UTM coordinate was originally taken and the Blue dots are the calculated locations of the map area boundaries. The pink outline in the center of the area defines a mound of gravel that had been moved there during placer mining operations.

3.2 Field Observations

Although the detailed study area is approximately level, it is within an area of past placer mining activity, and it was apparent that there had been a substantial amount of human disturbance that caused loose rock material to be displaced. Figure 6 shows the northern portion of the area where an excavator had moved rocks in a north-south direction.

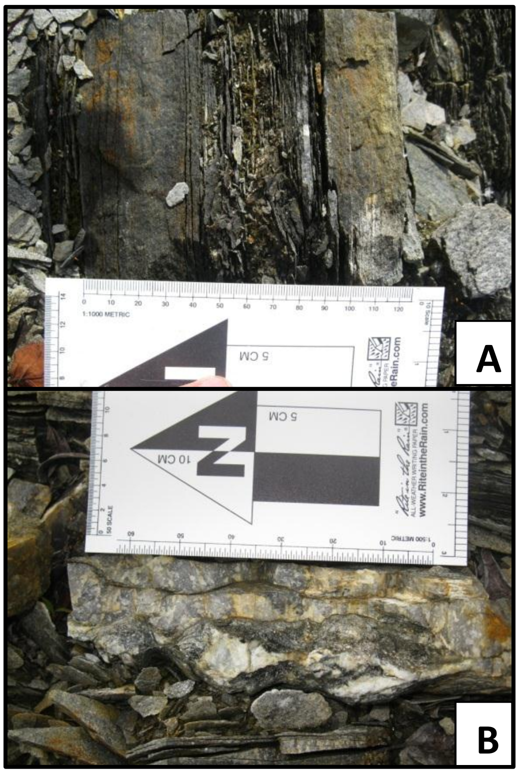

Figure 8: This figure shows two examples of the textural variations in the quartz – biotite schist. A is a photo of the thicker more competent rock enclosing bands of more fissile schist. B is a large quartz segregation with biotite concentrated along the margins.

Geological mapping for this project started in the northeast corner and continued south. From the first walk-through the dominant lithology was identified as a quartz-biotite schist with varying amounts of biotite; however, there were noticeable differences in the competency and amount of oxidation from one part of the area to the other. The northeast corner is underlain by a well foliated, fine grained quartz-biotite schist with very little evidence of surface weathering or hydrothermal alteration. This quartz-biotite schist grades into a more competent rock with larger quartz segregations, and tends to locally have a gossanous exterior. The quartz segregations are up to 4 cm thick with biotite concentrated along their boundaries (Fig 8B). Moving west, the quartz-biotite schist gradually changes into a medium-grained, moderately foliated rock with chlorite veins and oxidized fracture surfaces. Trace amounts of disseminated sulphide minerals are present in the northwestern section; however, they are too small to identify in hand sample

Moving south, there is a sharp contact between the quartz-biotite schist and a layer of micaceous quartzite. A total of three bleached quartzite layers occur in the northern section of the area (Fig. 6 and 7). Each layer has a true thickness of no more that than 2 meters. The foliation orientations are uniform across the three quartzite layers; nonetheless based on the map pattern these layers are interpreted to be limbs of a fold.

In the central part of the map area the quartz-biotite schist remains variable, with both the amount of biotite and the competency of the schist changing on a meter scale. There are no other occurrences of the bleached quartzite; however, a felsic dyke containing large, euhedral purple garnets occurs in this section. .

This dyke is irregular in character; locally it cross-cuts foliation whereas elsewhere it is parallel to the main foliation (Fig. 9A). The map pattern of the dyke suggests that it has been folded. Similarly locally derived boulders of the schist contain tight to isoclinal folds, although it was rare to find a fold that was in place. The dyke locally contains no garnets and displays a moderate foliation with 10%-15% aligned biotite.

Just to the south-east of this zone a gravel mound and flooding obscured part of the map area (Fig. 9B). On the south side of the flooded area large sections of white bull quartz are present within the quartz-biotite schist. These blebs of quartz create a complex map pattern that cannot be easily explained by the surrounding structure. The structure of this area consists of northwest-southeast striking foliations dipping 35°-42° to the southwest, which is quite different from that in the northern part of this southern section, where

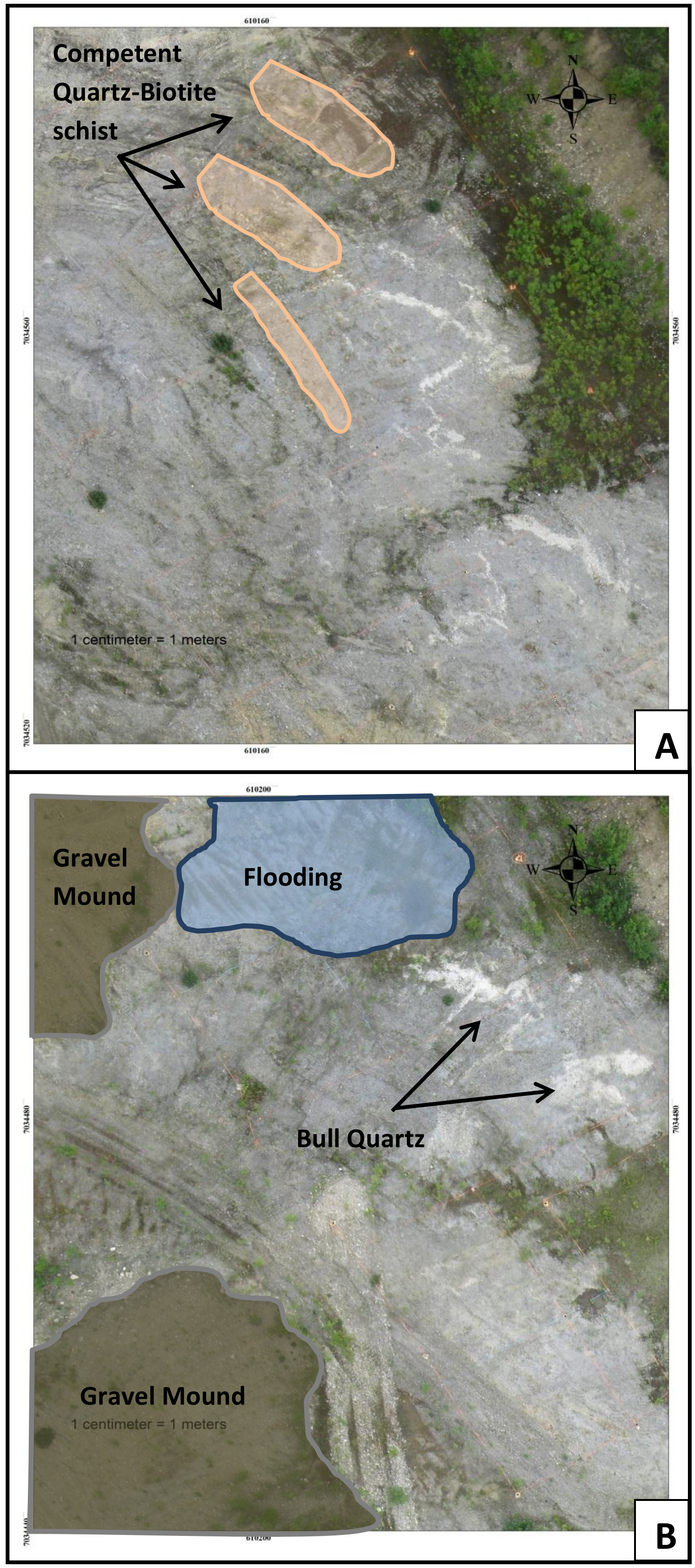

Figure 9: Photographs showing the central and southern section of the Black Hills Creek study area.

the dominant foliation is north-south striking and dips 10°-42° to the west.

3.3 Micaceous Quartzite

The micaceous quartzite unit is only found in the northern part of the study area, where it forms three sub-parallel layers, each with a true thickness of 1.5-3m. These rocks are moderately to well foliated, medium grained, and light grey to white in color. They consist of approximately `10% muscovite, 2% biotite, ~10% fine grained feldspar and 75%-80% quartz. They locally appear banded with a sugary-granular texture. The quartzite bands commonly display rusty weathering patches associated with oxidation of small irregular grains of iron sulphides to goethite and/or limonite.

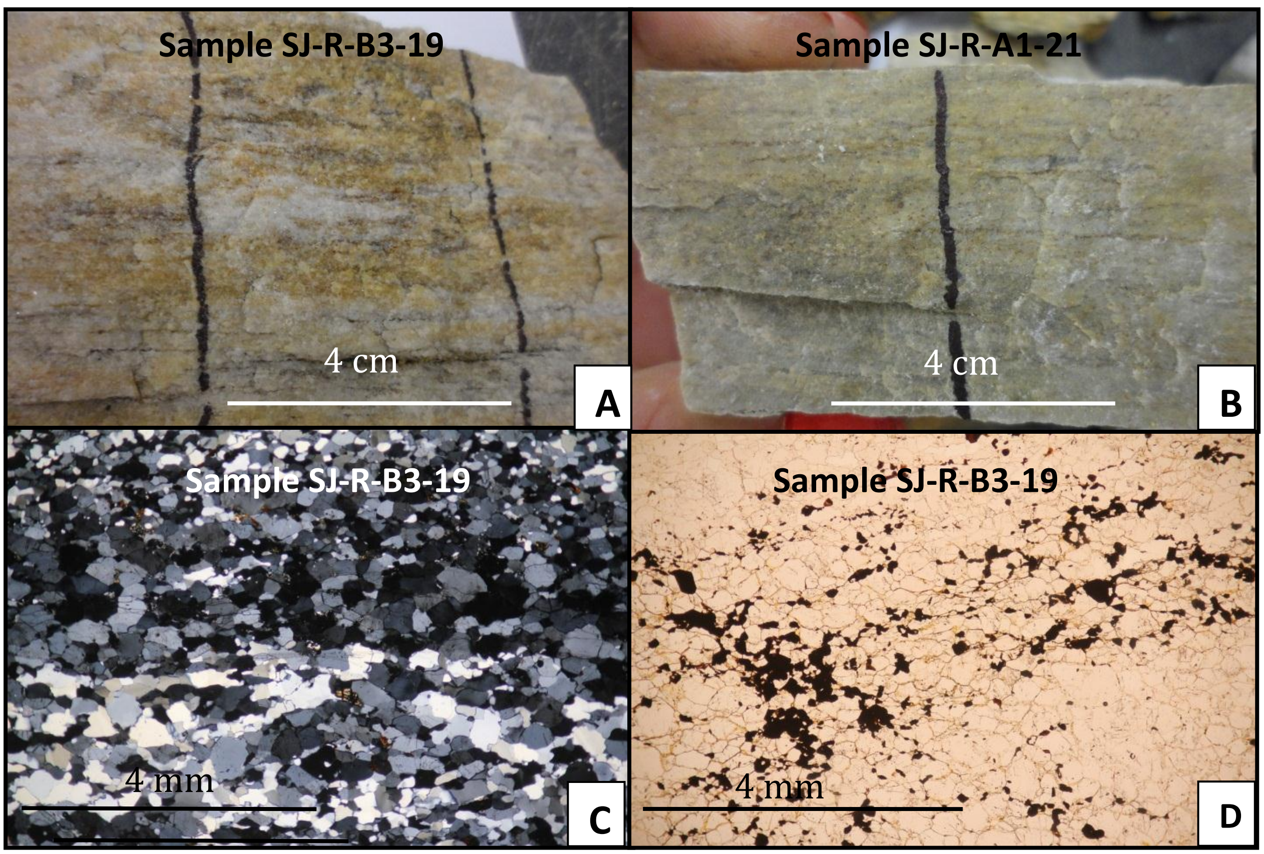

Figure 10: This figure shows photos of the micaceous quartzite from the northern part of the map area. A and B shows the variable texture of the quartzite and the type of oxidation that is common to this rock unit. Photo C is a photomicrograph in cross polarized light of the well foliated quartzite displaying sutured grain textures. Photo D, in plane polarized light, shows the amount of sulphide present in some portions of this rock. Most of these sulphides are now altered to limonite or goethite, displaying a reddish-brown colour surrounding the sulphide grains.

3.4 Quartz-Biotite-Muscovite (-Hornblende) Schist

This is one of the main units in the map area. In hand sample this unit can vary texturally on a meter scale. Figure 11 shows the location of three samples taken along a line cutting across the northern section of the map area. These three samples show the variation that can occur within a small zone. Sample B, the most easterly sample, is a light grey, fine grained metapelite. On weathered surfaces this rock develops a light tan-brown colour from the oxidizing biotite grains. It is well foliated with a high mica content (specific abundances are difficult to determine because of its fine grained nature). Sample B distinctly breaks into sheets 5-10mm thick. On the other hand, Sample C, located 4 meters to the southwest of sample B, fractures into irregular blocks. This sample is coarse grained with quartz segregations (on tens of mm scale) causing irregular fracturing.

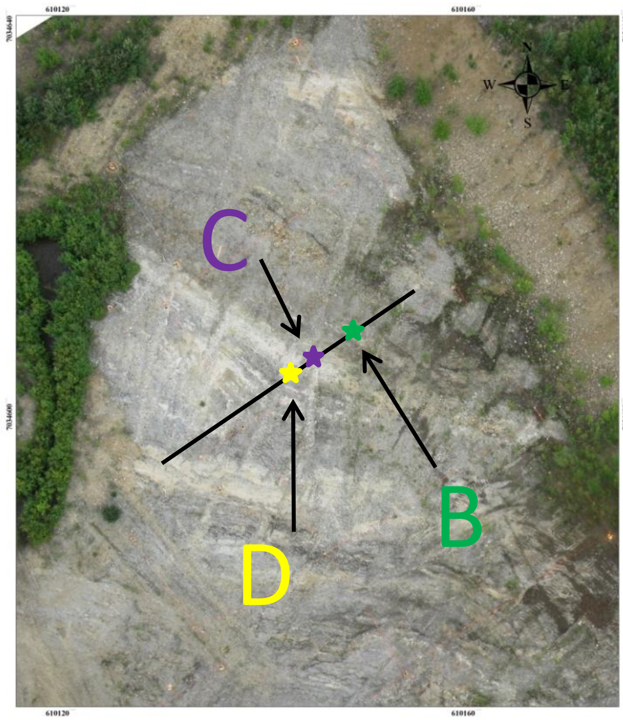

Figure 11: These three samples were taken along a 10 meter section of a line that cut the northern part of the map area from east to west. Sample B is a light grey-brown fine grained metapelite. Sample C is coarser grained with mm quartz segregations and Sample D is coarse grained, poorly foliated with 10%-20% micaceous material.

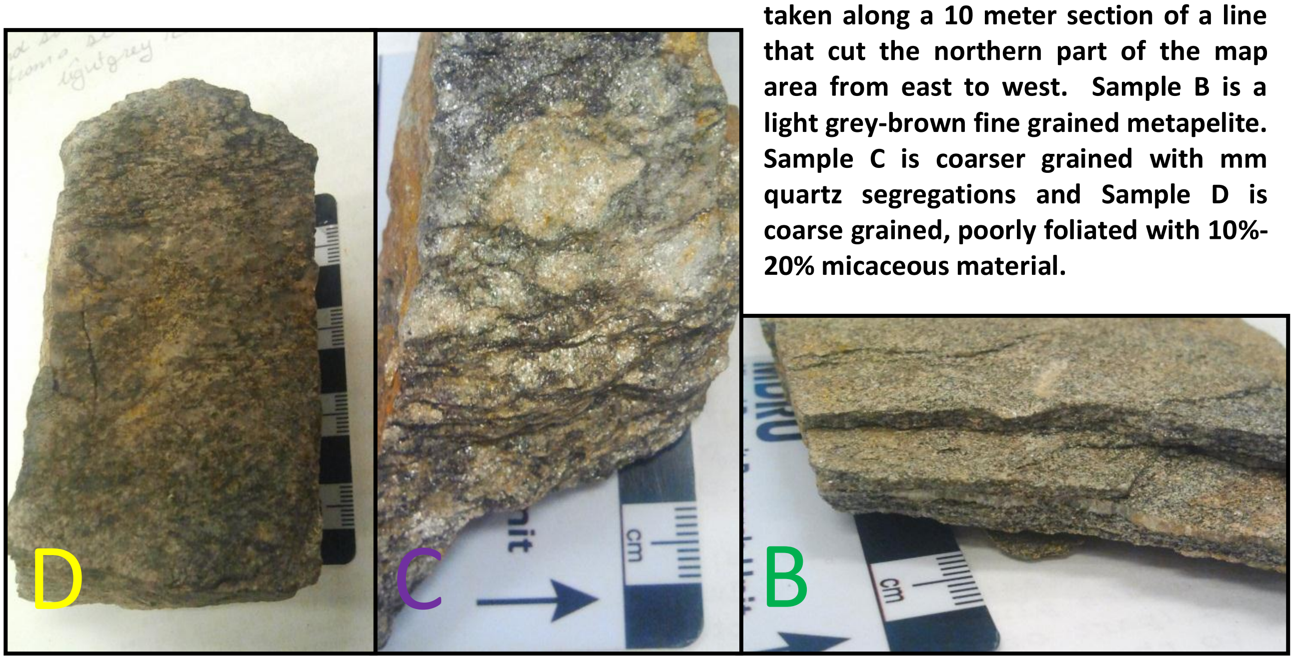

Along the fracture planes this schist has oxidized to a bright orange colour. This sample is still well foliated but lacks the strong schistosity observed in sample B. Conversely, sample D is poorly foliated. This sample is light to dark grey and is quartz rich compared to samples B and C. Sample D also lacks the oxidation along fractures as in Sample C and of the biotite in sample B. Variations of the type described here are visible throughout the entire map area and on a micro scale.

In thin section textual variation can be observed throughout the area; however, the schist shows consistent mineralogy. Figure 12 compares a sample taken from the southern section of the mapping area (SJ R-B11-4) to a sample from the central portion (SJ-R-B8-15). The schist unit is generally medium to coarse grained, containing 20%-30% fresh biotite. The quartz in the rock is a clear and dark grey in colour. There is commonly ~10%-15% muscovite present; however, this locally increases to almost 30% in some sections.

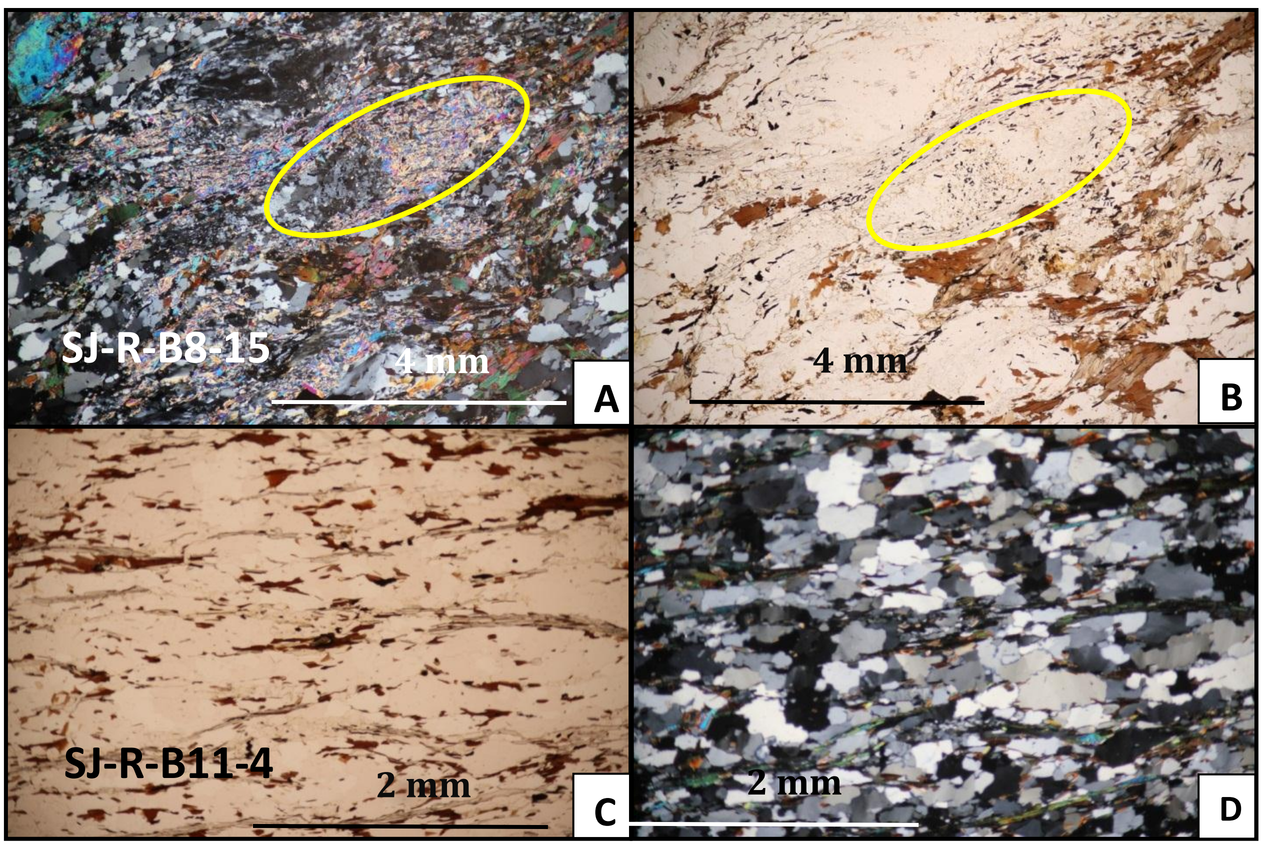

Figure 12: This figure above shows two samples of the quartz-biotite-muscovite schist from the southern and central parts of the map area. Sample SJ-R-B8-15, from the central region, shows a less well developed foliation with varying sizes of mica grains. In the centre of this photomicrograph there is a low birefringence mineral that appears to be partially replaced by muscovite. The minerals in this area have low relief and are thought to be either feldspar or cordierite. The other sample (SJ-R-B11-4, from the southern part of the map area) is well foliated, equigranular and does not contain the feldspar or cordierite minerals, which appear to have been replaced by muscovite.

The schist unit is locally oxidized throughout the map area; however, the oxidation is usually restricted to the more texturally competent variety of schist. The oxidation varies from yellowish (jarosite?) to dark brownish–red (goethite?). Lenses of very fissile material also occur locally within the more competent portion of the schists (Fig. 8). This textural change appears to be a product of an increase in mica content as well as a smaller grain size. Hornblende only occurs locally in this unit and observed in the northern area.

3.5 Felsic Dyke

The felsic dyke rocks show significant variability in composition and texture throughout the area. In some areas the dyke material is a massive leucocratic intrusive rock with large, purple, euhedral garnet on the order of 2mm-5mm in diameter (Sample SJ-D-A6-17), whereas elsewhere it is a foliated granitoid with 10%-15% biotite, containing less abundant and finer grained garnet (Sample SJ-D-A8-13).

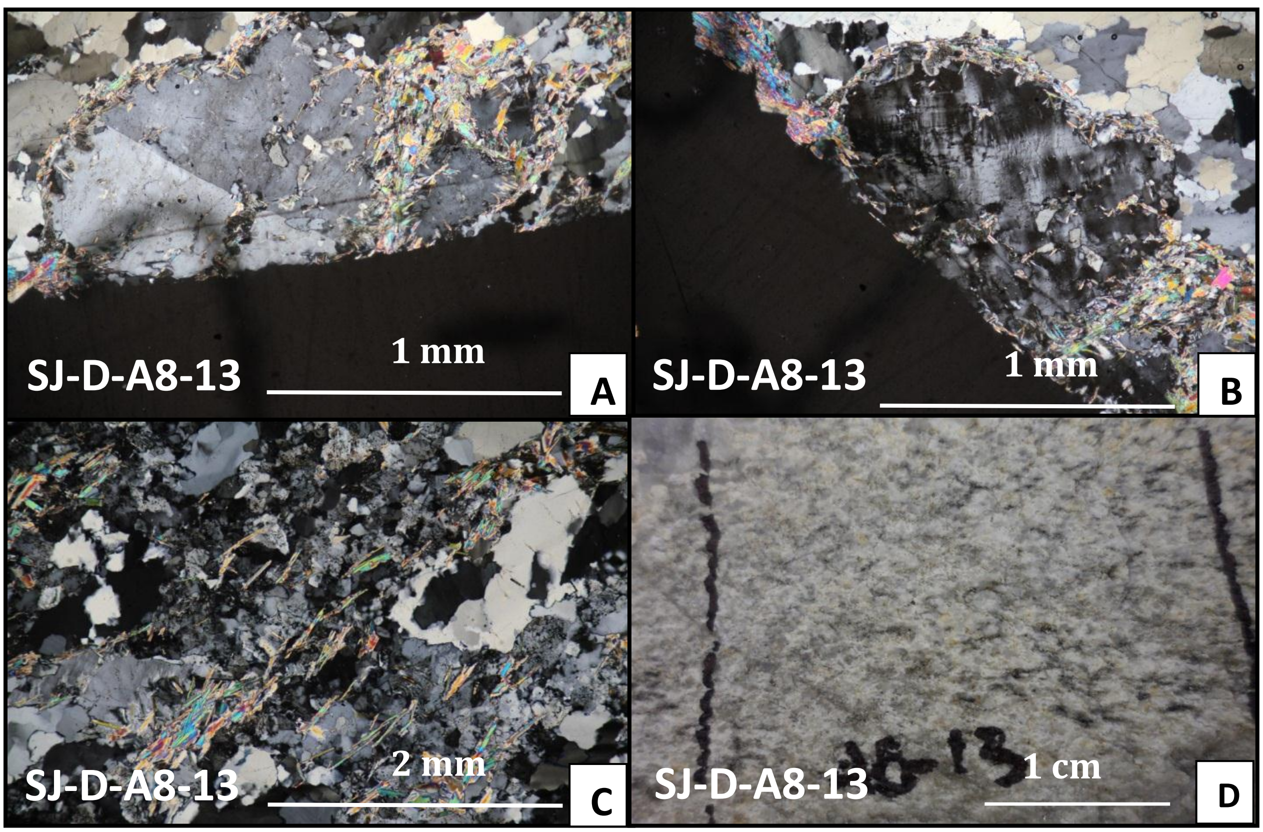

Figure 13: These photos show characteristics of the felsic dyke sample SJ-D-A8-13. A and B are photomicrographs illustrating the porphyroclastic texture of the feldspar phenocrysts that occur within this variety of the felsic dykes. Photographs C and D show the overall foliated nature of this sample.

Generally, the dykes are medium grained and comprise ~20%-25% quartz, ~25% plagioclase, ~30% potassium feldspar, ~15%-20% muscovite and locally 10%-15% biotite. The feldspars are commonly partially altered to sericite or clay minerals.

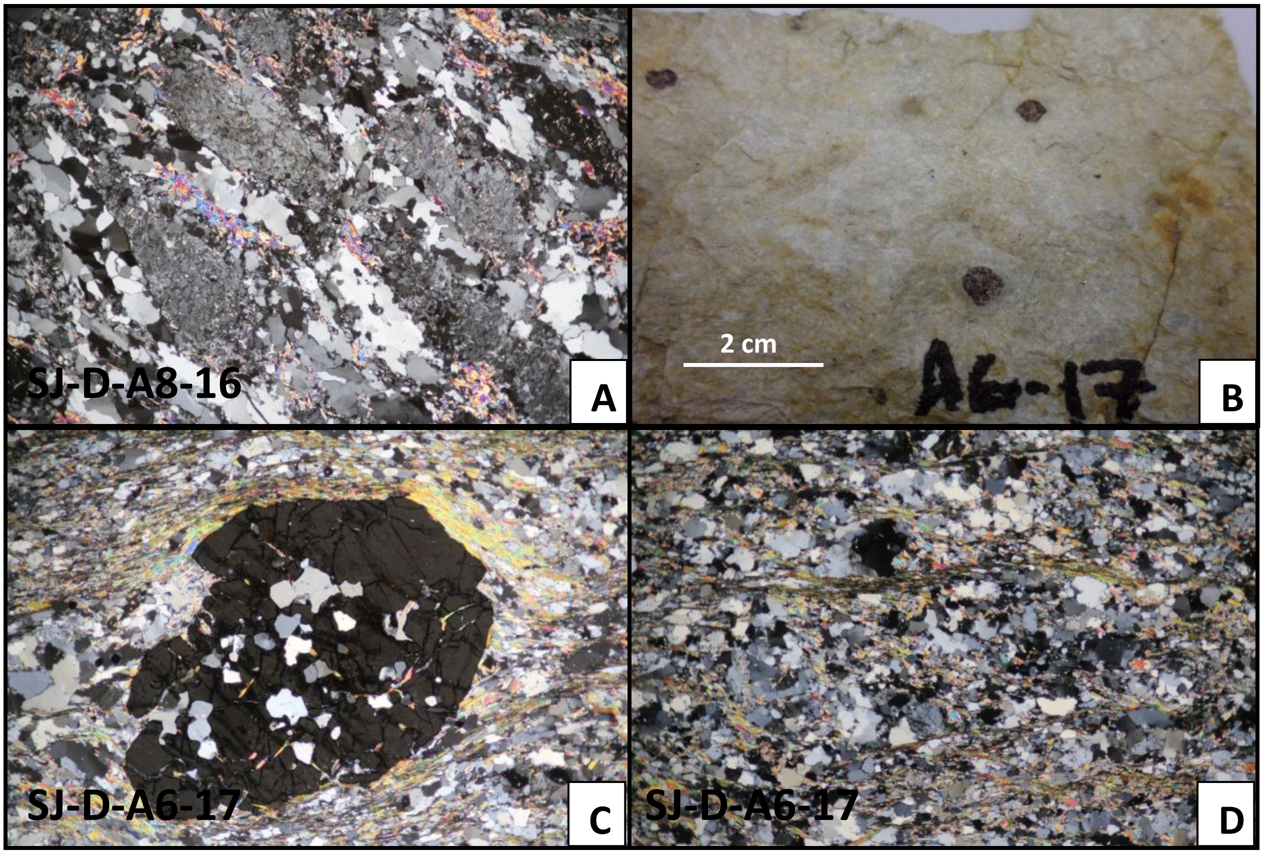

Figure 14: Photomicrograph A of sample SJ-D-A8-16 shows the alignment of feldspars in the felsic dyke. Photograph B and photomicrophs C and D are from the left limb of a folded felsic dyke in the central portin of the mapping area (Sample SJ-D-A6-17). This sample is the most distinctive with the large pre- to syn(?)-tectonic garnets. It is only weakly foliated compared to sample SJ-D-A8-13 but still contains abundant feldspar that is partially altered to sericite and/or clay.

3.6 Structural Analysis of Black Hills Creek Area

A structural analysis of the Black Hills Creek area was conducted to clarify the structural sequence preserved in the region and to ascertain the relationship between mineralization and deformation. A total of 84 structural measurements were taken as part of the detailed mapping study. The majority of these measurements are of pervasive foliation orientations, together with the some fold axis measurements (Plate 1).

The pervasive foliation generally strikes NW-SE and shallowly dips (<40°) to the SW. This foliation is mostly consistent throughout the area with locally steeper dips and more north-south striking fabrics. The felsic dykes cross cut this pervasive foliation at a shallow angle (~20°). Locally the dyke material contains a weak fabric, defined by aligned biotites and feldspars that are parallel to the pervasive foliation found in the quartz-biotite schists. The schists and dykes have subsequently been folded by mainly horizontal, upright to overturned, tight to isoclinal folds that trend NW-SE, parallel to pervasive foliation (Fig. 17)

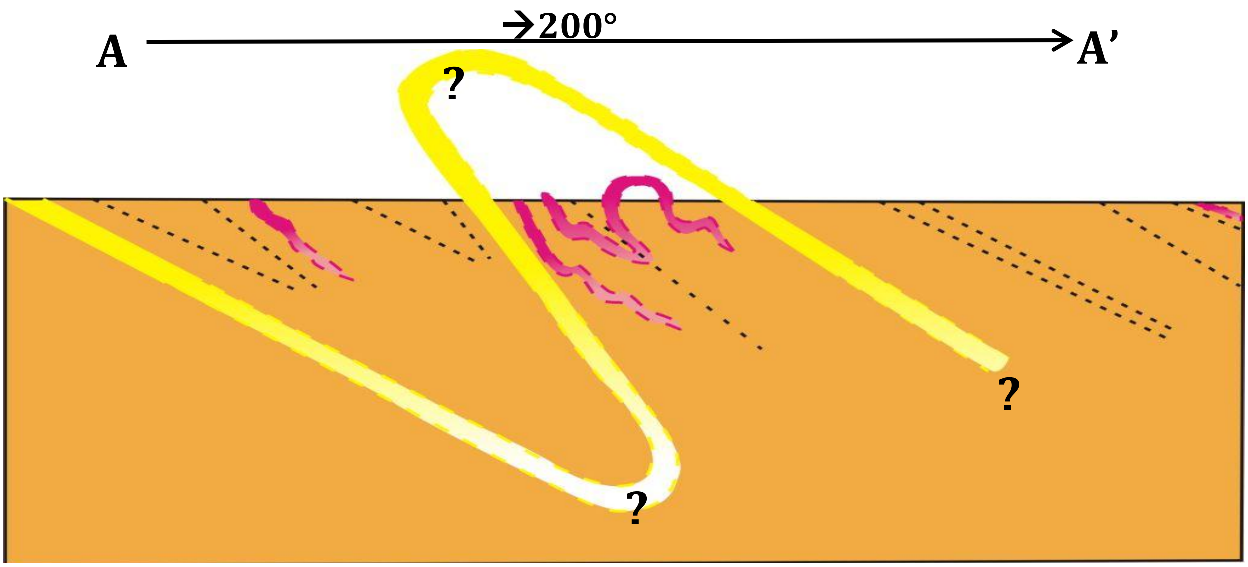

Figure 15: Cross section A-A' in the northern section of the mapping area. It has been inferred that the deformed quartzites (yellow) have been folded with an axial surface parallel to pervasive foliation (black dashed lines). The pink units represent the folded dykes in the hinge of the fold

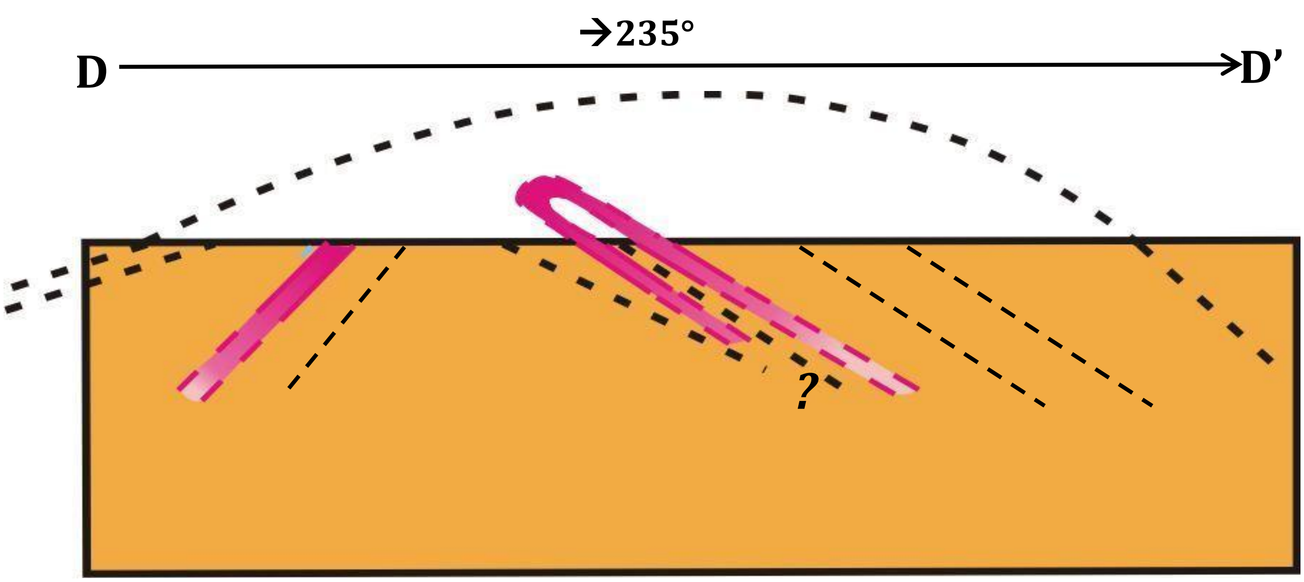

Figure 16: Cross section D-D' is an open fold that deforms the dominant schistosity in the central part of the mapping area. The exact geometry of the felsic dykes within the core of the fold is uncertain.

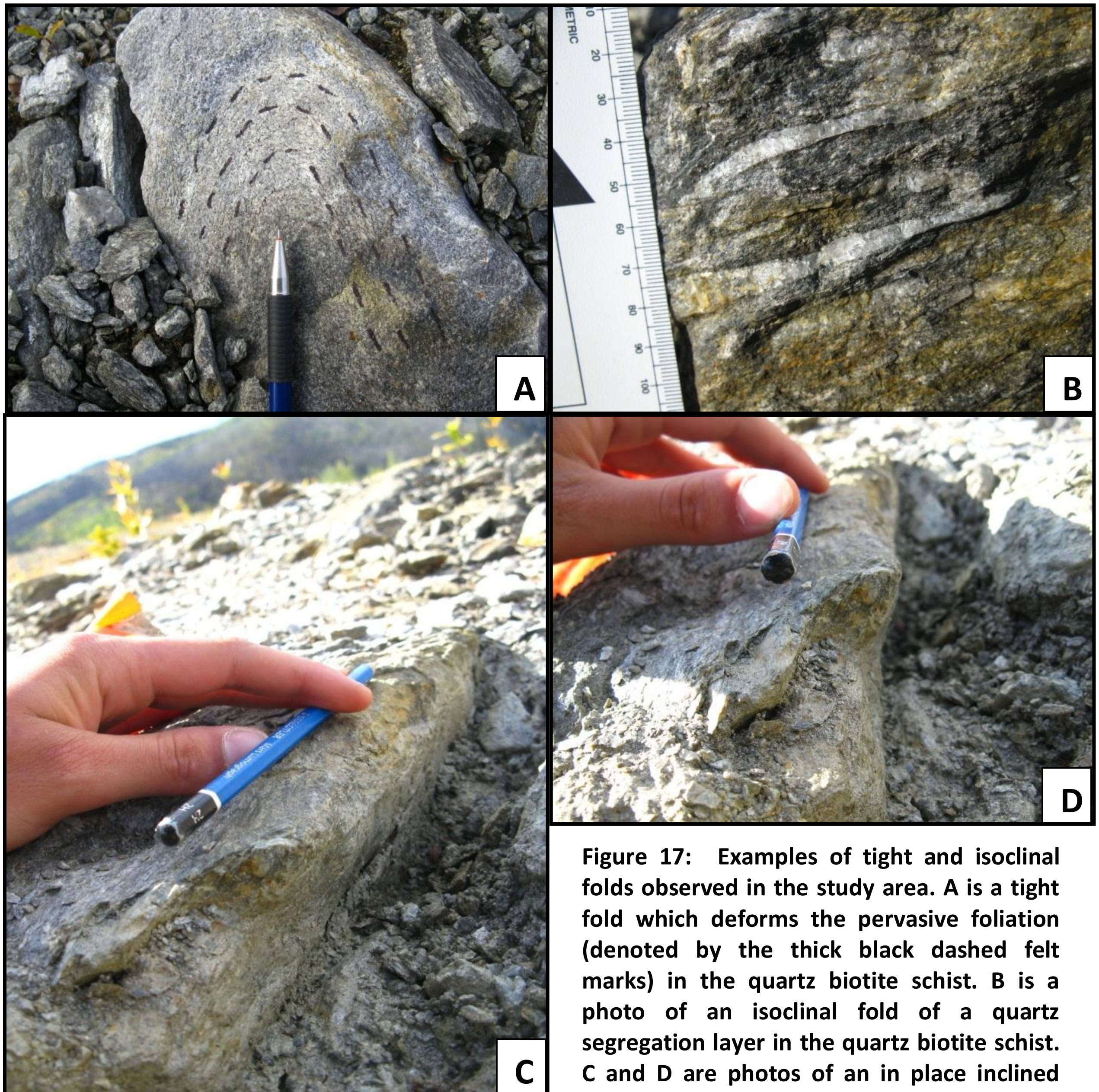

Figure 17: Examples of tight and isoclinal folds observed in the study area. A is a tight fold which deforms the pervasive foliation (denoted by the thick black dashed felt marks) in the quartz biotite schist. B is a photo of an isoclinal fold of a quartz segregation layer in the quartz biotite schist. C and D are photos of an in place inclined isoclinal fold trending NW-SE and verging to the NE.

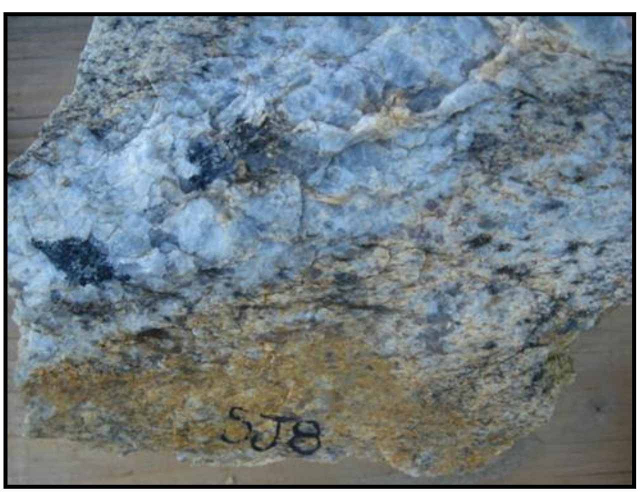

Figure 18: A quartz vein with euhedral tourmaline crystals cross cutting a foliated felsic dyke.

There are two generations of quartz veins that can be traced throughout the mapping area. The first generation consists of a greyish-blue quartz, and is observed cross-cutting the felsic dykes (Fig.18), whereas the second generation, comprising white quartz, is more commonly found along the felsic dyke contacts with the host rock. Neither of the veins type is solely associated with the felsic dyke, however; they are distributed through the mapping area.

Chapter 4

4.1 Geochemical Analysis

Geochemical analysis was considered to be an important aspect of this field study based on the field relationships and rock compositions found in the Black Hills Creek area. The rock compositions of the felsic dykes had similar characteristics to other Late Permian and Early Jurassic felsic intrusives found in the western Yukon, therefore it was considered most likely that these dykes would be of similar age to one of these two magmatic pulses. The geochemical data was plotted against a large dataset of Early Jurassic intrusions and a sample of the Permian Jim Creek pluton from the Aldrin IND property in the western Yukon. Three samples of the felsic dyke found in the study area were chosen to ensure a comprehensive analysis was done on all compositional and textural variations of the dyke. A fourth sample of the "quartzite" unit was analyzed to help ascertain the protolith. In the field this unit was referred to as a micaceous quartzite; however, microscopy revealed feldspar was present, raising the possibility that this unit might have a felsic volcanic protolith.

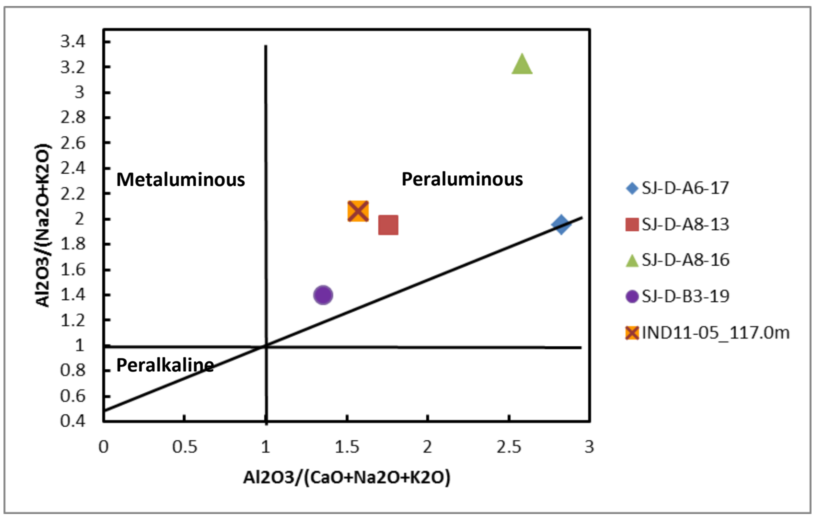

Figure 19: The Shaud plot (Shaud,1943) discriminates between peralkaline, metaluminous and peraluminous compositions of igneous rocks. All four samples from Black Hills Creek fall well within the peraluminous field similarily sample IND11-05_177.0m is a fresh sample of the Jim Creek Pluton from the Aldrin IND property.

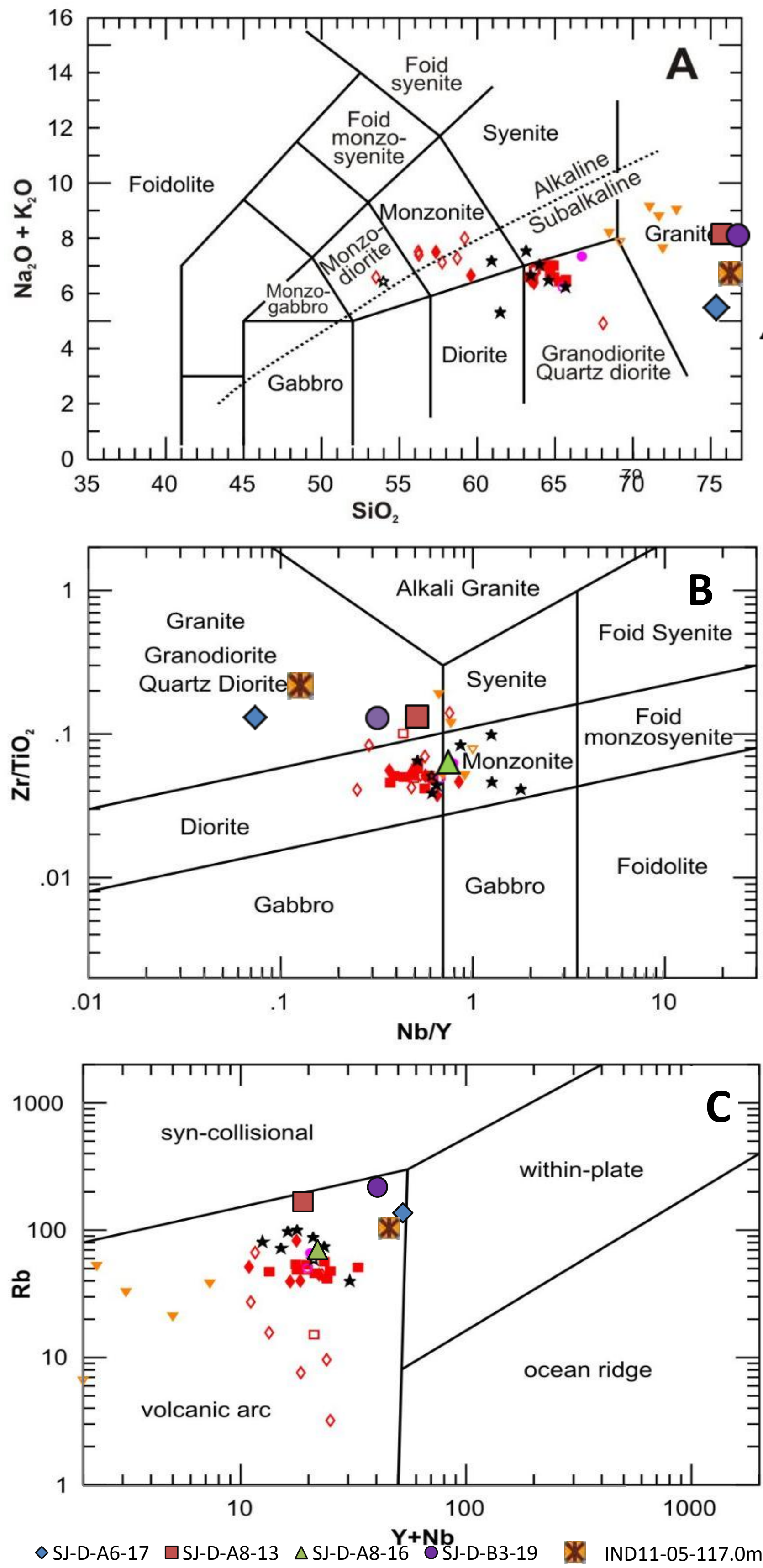

Whole rock chemical analyses and hand sample photographs of the three representative samples of the felsic dyke from the study area (samples SJ-D-A6-17, SJ-D-B3-14, and SJ-D-A8-16) and one of the "quartzite" (possible felsic metavolcanic rock; sample SJ-D-B3-19) are given in Appendix C. Although there are a limited number of samples from the study area, they are compared with other felsic intrusive phases in western Yukon to test possible geochemical similarities

Figure 20: The results showing the overall granitic compositions of the felsic dyke in the Black Hills Creek area compared with samples of plutonic rocks of the Minto and Williams Creek areas and and Granite Mountain Batholith (small symbols). A is a total alkali vs. SiO_2 plot defining the samples as subalkaline intrusions (discriminant of Irvine and Barager, 1971). B is an immobile element ratio plot after Winchester and Floyd (1977). C breaks plutonic rocks in terms of tectonic setting signatures.

with suits of known age and tectonic setting. The samples are compared to Early Jurassic intermediate to felsic intrusive rocks from the Minto and Williams Creek areas, the Granite Mountain batholith in the eastern Dawson Range and the Jim Creek Pluton ~50km SSW of Dawson (Fig.19 and 20).

On a total alkalis vs. SiO_2 plot, after Le Bas *et al.* (1986), all four samples plot in the granite field. As seen in Figure 20A the dyke samples from the study area are considerably more felsic than the Minto and Williams Creek samples which fall mostly in the granodiorite/quartz diotite to monzodiorite fields. All samples from the study area show subalkaline compositions (discriminant of Irvine and Baragar, 1971; Fig. 20A) and they all yield peraluminous compositions (Fig. 19). However, it is uncertain how much this reflects primary igneous compositions and to what extent hydrothermal alteration and/or metamorphism compositions. For example, sample SJ-D-A8-16 is a sample of the felsic dyke from a region close to sample SJ-D-A8-13 and yet plots much farther into the peraluminous field.

Figure 20B displays an immobile element ratio plot (Nb/Y vs Zr/TiO_2) after Winchester and Floyd (1977). The well foliated felsic dyke samples (SJ-D-A8-13), the garnet bearing felsic dyke sample (SJ-D-A6-17) and the "quartzite" sample fall in the granite/granodiorite/quartz diorite field, whereas sample SJ-D-A8-16 yields a more monzonitic composition. The samples all plot within the volcanic arc field on a Y+Nd vs. Rb plot (Fig. 20C; after Pearce *et al.*, 1984) but three of the four samples lie close to the borders of the syn-collisional and within plate fields.

From the geochemical analysis conducted, the felsic dyke samples from the Black Hills Creek area resembles a more felsic volcanic arc intrusive than those of the Minto and Williams Creek areas. The dyke geochemistry suggests it is a peraluminous granite. Similarly, the geochemistry of the "quartzite" sample suggests it is has a felsic igneous composition and probably represents a felsic metavolcanic protolith. This sample is compositionally similar to the three dyke samples falling within the volcanic arc field, being peraluminous and seemingly granitic in composition. Field relationships, however, indicate that the "quartzite" unit is part of the metamorphic basement package in the Black Hills Creek area, and must be older than and unrelated to the felsic dyke.

A total of 14 samples were sent for metallurgical assay analysis however no significant values for gold or silver recovered. These analyses can be found in Appendix D.

4.2 U-Pb Geochronology

U-Pb dating was used to attempt to constrain the ages of protoliths of some of the rock units in the study area as well as the age of the main stage of metamorphism and deformation that affected them. Metamorphic monazite was separated from two samples of the main biotite schist unit. Monazite was recovered from one felsic dyke sample and zircons were recovered from a second dyke sample. Monazite was analyzed from the two schist samples and from one dyke sample, all using conventional ID-TIMS methods. Two single grain zircon analyses were done for the second dyke sample using the chemical abrasion (CA)-TIMS method.

4.3 U-Pb Analytical Techniques

Chemical abrasion (CA) TIMS procedures for U-Pb analysis of zircons are described here (modified from Mundil *et al*., 2004, Mattinson, 2005, and Scoates and Friedman, 2008). After rock samples have undergone standard mineral separation procedures zircons and monazites are handpicked in alcohol. The clearest, crack- and inclusion-free zircon grains are selected, photographed and then annealed in quartz glass crucibles at 900˚C for 60 hours. Annealed grains are transferred into 3.5 mL PFA screwtop beakers, ultrapure HF (up to 50% strength, 500 mL)

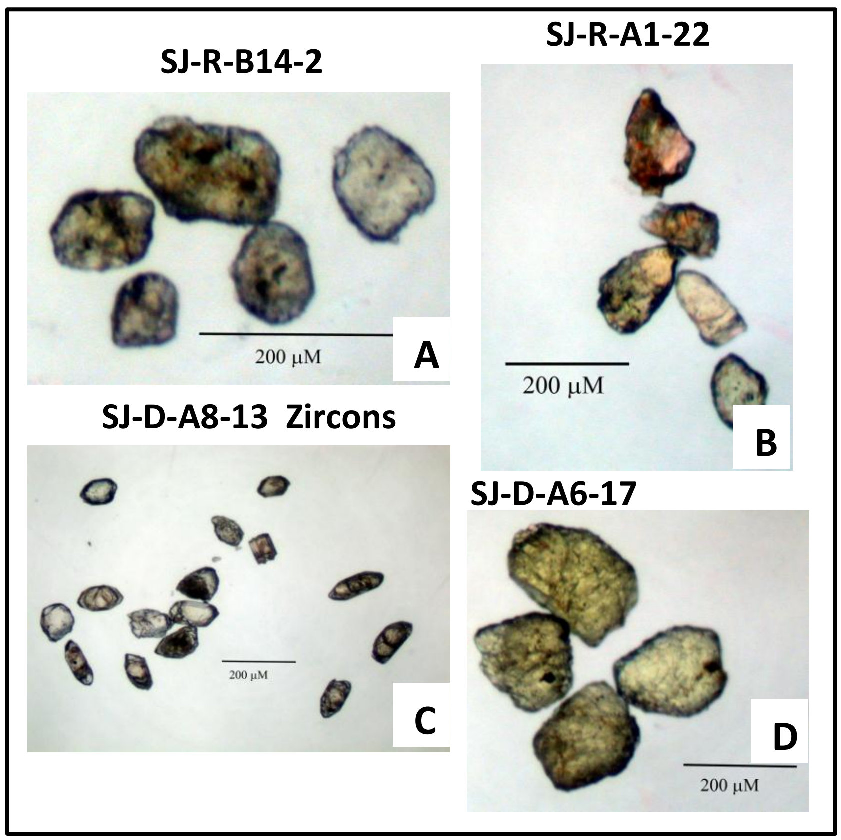

Figure 21: Photomicrographs of the U-Pb samples. A shows the poorly formed monazites recovered from the quartz-biotite schist sample SJ-R-B14-2. B exhibits the monazites picked from the second schist sample (sample SJ-R-A1-22) C shows the zircons recovered from the garnet-poor felsic dyke, sample SJ-D-A8-13. Lastly, D shows the poor quality monazites recovered from the garnet bearing felsic dyke sample (SJ-D-A6-17).

and HNO3 (up to 14 N, 50 mL) are added and caps are closed finger tight. The beakers are placed in 125 mL PTFE liners (up to four per liner) and about 2 mL HF and 0.2 mL HNO3 of the same strength as acid within beakers containing samples are added to the liners. The liners are then slid into stainless steel Parr™ high pressure dissolution devices, which are sealed and brought up to a maximum of 200˚C for 8-16 hours (typically 175˚C for 12 hours). Beakers are removed from liners and zircon is separated from leachate. Zircons are rinsed with >18 MΩ.cm water and subboiled acetone. Then 2 mL of subboiled 6N HCl is added and beakers are set on a hotplate at 80˚-130˚C for 30 minutes and again rinsed with water and acetone. Masses are estimated from the dimensions (volumes) of grains. Single grains are transferred into clean 300 mL PFA microcapsules (crucibles), and 50 mL 50% HF and 5 mL 14 N HNO_3 are added. Each is spiked with a $^{233\text{-}235}$U-^{205}Pb tracer solution (EARTHTIME ET535), capped and again placed in a Parr liner (8-15 microcapsules per liner). HF and nitric acids in a 10:1 ratio, respectively, are added to the liner, which is then placed in Parr high pressure device and dissolution is achieved at 240˚C for 40 hours.

The resulting solutions are dried on a hotplate at 130˚C, 50 mL 6N HCl is added to microcapsules and fluorides are dissolved in high pressure Parr devices for 12 hours at 210˚C. HCl solutions are transferred into clean 7 mL PFA beakers and dried with 2 mL of 0.5 N H_3PO_4. Samples are loaded onto degassed, zone-refined Re filaments in 2 mL of silicic acid emitter (Gerstenberger and Haase, 1997). Monazite grains are not analyzed using the chemical abrasion method that is described above for zircons. Instead, clean, acid-washed single grains of monazite are dissolved in the presence of the same isotopic tracer as is used for zircon, but in ultrapure concentrated HCl.

Isotopic ratios are measured using a modified single collector VG-54R or 354S (with Sector 54 electronics) thermal ionization mass spectrometer equipped with analogue Daly photomultipliers. Analytical blanks are 0.2 pg for U and 1 pg for Pb. U fractionation was determined directly on individual runs using the EARTHTIME ET535 mixed 233-235U-205Pb isotopic tracer and Pb isotopic ratios were corrected for fractionation of 0.23%/amu, based on replicate analyses of NBS-982 reference material and the values recommended by Thirlwall (2000). Data reduction employed the excel-based program of Schmitz and Schoene (2007). Standard concordia diagrams were constructed and regression intercepts, weighted averages calculated with Isoplot (Ludwig, 2003). Unless otherwise noted all errors are quoted at the 2 sigma or 95% level of confidence. Isotopic dates are calculated with the decay constants for ^{238}U = 1.55125E-10 and for ^{235}U = 9.8485E-10 (Jaffe et al., 1971). EARTHTIME U-Pb synthetic solutions are analysed on an on-going basis to monitor the accuracy of results.

4.4 U-Pb Analytical Results

Monazite recovered from the biotite schist unit forms irregular subsequent grains with poor crystal form (Fig. 21A). Two grains of monazite from one of the schist samples (samples R-B14-22) give overlapping nearly concordant U-Pb analyses (Table 2, Fig. 22A). Monazite contains very high Th contents and hence in some cases contains trace to substantial amounts of excess disequilibrium ^{206}Pb, which commonly results in monazite analyses plotting slightly above the concordia curve. In order to avoid this complication the $^{207}Pb/^{235}U$ age is generally taken as the best estimate for the crystallization age of the monazite. A weighted average $^{207}Pb/^{235}U$ age of 260.7 ±1.1 Ma for these two monazite analyses is interpreted to date peak metamorphism in the host schists in this area. This age is consistent with the estimate for the age of the Klondike orogeny (260-252.5 Ma) as constrained by Beranek and Mortensen (2011). A single grain of monazite from the second schist samples (sample SJ-R-A1-22; Fig.20B) lies above concordia and gives a considerably younger age of 248.1 ±0.8 Ma (Table 2; Fig. 22A). The significance of this analysis is unclear. It could either indicate that the schist unit remained deeply buried at high enough temperature that monazite continues to grow until at least 248.1 Ma, or could reflect a second, slightly younger metamorphic event. Berman *et al.* (2007) reported U-Pb age data for samples in the Stewart River map area that they interpreted to indicate growth of metamorphic zircon and monazite in the area over an extended period from ~260 to 239 Ma.

The felsic dykes in the study area crosscut and therefore postdate the main metamorphic fabric in the host schists. The dykes locally contain a metamorphic fabric, however, suggesting that they may have been emplaced at a relatively late stage during a protracted period of deformation and metamorphism after the Klondike orogeny. In any case the age of the dykes must be younger than the main stage of deformation and metamorphism associated with the

Klondike orogeny, which is presumed to be given by the U-Pb monazite age of 260.7 Ma from the first schist samples.

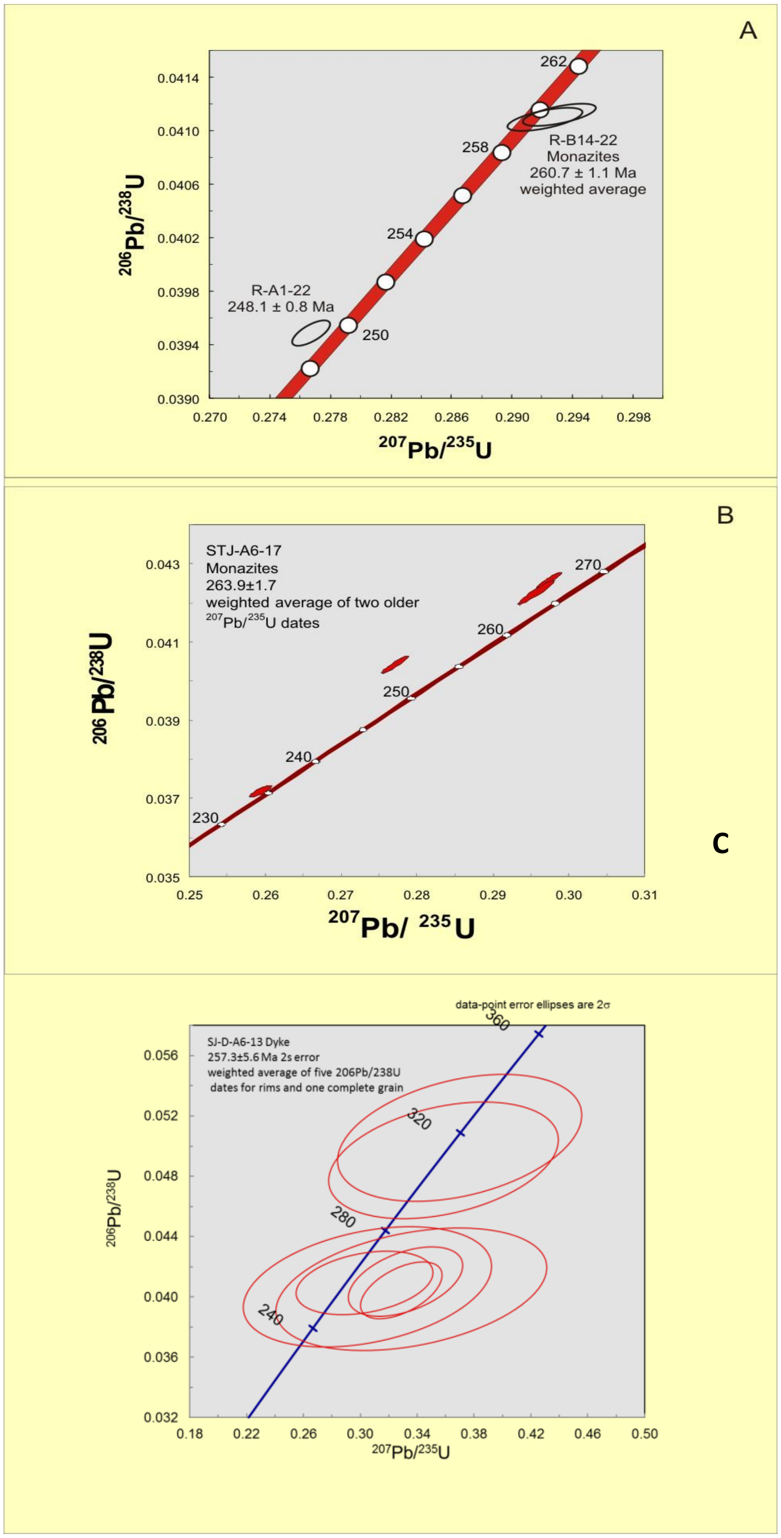

Figure 22: This figure shows the U-Pb results from the U-Pb analysis of samples SJ-D-A6-17, SJ-R-B14-22 and sample SJ- R-A1-2.

A small amount of fine-grained zircon was recovered from a relatively garnet-poor felsic dyke sample (sample SJ-D-A8-13; Fig. 21C). Most of the grains contained large rounded cores and in some grains only a very thin euhedral rim was present. This was interpreted to indicate that most of the zircons represented old inherited cores derived from the source rock and that only a thin igneous rim was present in most grains. Three single zircon grains were analyzed; however, only two fractions yielded usable results (Table 2). One fraction yielded a strongly discordant analysis (Fig. 22A), consistent with being a mixture of an older inherited core and a younger igneous overgrowth. A second analysis yielded a concordant analysis with an age of 321.5 Ma (Fig. 22B). The significance of this age is uncertain. Since it is older than the possible upper limit of possible emplacement age for the dyke, this zircon fraction must have been a xenocryst or an igneous overgrowth around an inherited zircon core that was only slightly older. There are no known ~322 Ma igneous rocks in the western Yukon, so it is unlikely that the zircon grain is a xenocryst. Because the analysis is concordant, it could conceivably be a mixture of slightly older zircon core (345.4-360 Ma metaplutonic rocks are known to be widespread in this area) and a younger (<260.7 Ma) igneous rim. A second zircon gave a concordant analysis 257.3 ±5.6 Ma. This younger date is consistent with the felsic dykes intruding after the main metamorphic event ~260 ma

Monazite grains recovered from the second, garnet-rich dyke sample (sample SJ-D-A6-17) are generally similar in appearance to those from the schist samples, with relatively poor clarity and poor crystal form (Fig. 21D). Four single monazite grains were analyzed from the sample (Table 2, Fig 22B). Two grains give identical ages with a weighted average of 263.±1.7 Ma. This is older than the interpreted age of the main metamorphic event that affected the schists and therefore older than the dyke itself. These monazite grains are interpreted to be xenocrysts that were entrained from deeper metamorphic wall rocks. One fraction of monazite gives a $^{207}Pb/^{235}U$ age of 248.2 ±0.8 Ma, which is very similar to the age obtained from one of the monazite grains from the second schist sample. A fourth monazite grain gave a still younger age of 234.2 ± 1.0 Ma.

The age of the felsic dykes in the study area has not been fully resolved by the U-Pb dating thus far. Based on regional correlations it is thought most likely that the dykes are part of the latest Permian suit of crustally derived granites, which include the Jim Creek pluton, that were emplaced late in the Klondike orogeny. The U-Pb data are mostly compatible with the interpretation, except for the single monazite fraction from the one dyke sample that gave an age of 232 Ma. More work is planned to attempt to better resolve the age of the dykes.

Table 2: Is the Monazite and zircon U-Th-Pb isotopic data for the different fractions of samples SJ-D-A6-17, SJ-R-A1-22, Sj-R-B14-22 and sample SJ-D-A8-13

Table 2. Monazite and zircon U-Th-Pb isotopic data.

	Compositional Parameters									Radiogenic Isotope Ratios								Isotopic Ages					
Sample	Wt. mg	U ppm	$\frac{Th}{U}$	Pb ppm	$^{206}Pb^*$ x10^{-13} mol	mol % $^{206}Pb^*$	$\frac{Pb^*}{Pb_c}$	Pb_c (pg)	$\frac{^{206}Pb}{^{204}Pb}$	$\frac{^{208}Pb}{^{206}Pb}$	$\frac{^{207}Pb}{^{206}Pb}$	% err	$\frac{^{207}Pb}{^{235}U}$	% err	$\frac{^{206}Pb}{^{238}U}$	% err	corr. coef.	$\frac{^{207}Pb}{^{206}Pb}$	±	$\frac{^{207}Pb}{^{235}U}$	±	$\frac{^{206}Pb}{^{238}U}$	±
(a)	(b)	(c)	(d)	(c)	(e)	(e)	(e)	(e)	(f)	(g)	(g)	(h)	(g)	(h)	(g)	(h)		(i)	(h)	(i)	(h)	(i)	(h)
ST-D-A6-17 Monazite																							
M1	0.028	2970	6.457	303.8	128.0749	97.74%	33	####	808	2.038	0.050613	0.251	0.259386	0.459	0.037169	0.337	0.844	223.25	5.80	234.17	0.96	235.26	0.78
M2	0.027	2855	6.391	324.0	136.9000	98.97%	74	117.34	1785	1.990	0.050676	0.159	0.297383	0.449	0.042561	0.388	0.938	226.10	3.68	264.35	1.04	268.69	1.02
M3	0.012	3171	6.396	360.8	65.9631	98.36%	46	90.70	1119	1.997	0.050764	0.213	0.295685	0.667	0.042245	0.608	0.948	230.13	4.93	263.02	1.55	266.73	1.59
M4	0.011	3641	6.563	397.3	66.9101	98.74%	60	70.73	1450	2.021	0.049732	0.181	0.277068	0.525	0.040406	0.464	0.941	182.49	4.21	248.33	1.16	255.35	1.16
SJ-R-A1-22 Monazite																							
M1	0.0026	2754	6.389	290.3	11.7967	99.40%	128	5.85	3074	2.012	0.050831	0.269	0.276735	0.370	0.039485	0.198	0.708	233.17	6.21	248.06	0.81	249.64	0.48
SJ-R-B14-2 Monazite																							
M1	0.0019	2808	6.489	325.9	9.1465	96.31%	20	29.00	488	2.061	0.051584	0.603	0.292211	0.693	0.041084	0.163	0.632	267.03	13.84	260.30	1.59	259.55	0.42
M2	0.0027	2109	5.517	222.5	9.7667	96.15%	18	32.37	469	1.756	0.051709	0.582	0.293153	0.671	0.041117	0.164	0.630	272.58	13.33	261.04	1.54	259.75	0.42
SJ-D-A6-A13 Zircon																							
A	0.0010	293	0.562	86.7	2.6165	99.25%	52	1.62	2463	0.307	0.267621	0.102	7.895838	0.218	0.213981	0.136	0.938	3292.14	1.60	2219.20	1.97	1249.99	1.55
B	0.0020	774	0.288	39.7	3.3032	99.44%	51	1.53	3297	0.091	0.052796	0.170	0.372314	0.267	0.051145	0.139	0.832	320.05	3.86	321.37	0.74	321.55	0.44

(a) A, B etc. are labels for fractions composed of single chemically abraded grains and M1, M2 for single monazite grains with no pre-treatment.

(b) Nominal fraction weights estimated from photomicrographic grain dimensions.

(c) Nominal U and total Pb concentrations subject to uncertainty in photomicrographic estimation of weight.

(d) Model Th/U ratio calculated from radiogenic 208Pb/206Pb ratio and 207Pb/235U age.

(e) Pb* and Pbc represent radiogenic and common Pb, respectively; mol % $^{206}Pb^*$ with respect to radiogenic, blank and initial common Pb.

(f) Measured ratio corrected for spike and fractionation only. Mass discrimination of 0.23%/amu based on analysis of NBS-982; all Daly analyses.

(g) Corrected for fractionation, spike, and common Pb; up to 10 pg (monazite) and 1pg (zircon) of common Pb was assumed to be procedural blank: 206Pb/204Pb = 18.50 ± 1.0%; 207Pb/204Pb = 15.18 ± 1.0%; 208Pb/204Pb = 38.40 ± 1.0% (all uncertainties 1-sigma). Excess over blank was assigned to initial common Pb with S-K model Pb composition at the age of the grain.

(h) Errors are 2-sigma, propagated using the algorithms of Schmitz and Schoene (2007) and Crowley et al. (2007).

(i) Calculations are based on the decay constants of Jaffey et al. (1971). 206Pb/238U and 207Pb/206Pb ages corrected for initial disequilibrium in 230Th/238U using Th/U [magma] = 3.

4.5 Sulphide Lead Isotopes: Analytical Techniques and Results

Sulphide samples from various areas in the mapping area were analyzed using a modified VG54R thermal ionization mass spectrometer operating in peak-switching mode on a Faraday detector. Sample preparation, geochemical separation and isotopic analysis were conducted at the PCIGR facility at the University of British Columbia. Approximately 10-50 milligrams of sulphides from each sample were handpicked, and then leached in dilute hydrocholoric acid to remove all surface and other sources of contamination. The sulphides were then dissolved in diluted nitric acid. Following dissolution approximately 100-250 nanograms of Pb in chloride form was loaded on rhenium filaments using a phosphoric acid-silica gel emitter and analyzed. The isotopic ratios were corrected for instrumental mass fractionation of 0.12%/amu based on repeated measurements of the NBS 981 Pb standard and the values recommended by Thirwall (2000). Table 3 reports the isotopic analyses with errors reported at the 2 sigma level.

Table 3: Lead isotopic compositions for pyrite from veins in the Black Hills Creek area.

Sample Number	Mineral	$^{206}Pb/^{204}Pb$	Error %2 sigma	$^{207}Pb/^{204}Pb$	Error %2 sigma	$^{208}Pb/^{204}Pb$	Error %2 sigma	$^{207}Pb/^{206}Pb$	Error %2 sigma	$^{207}Pb/^{206}Pb$	Error %2 sigma
SJ-R-A9-11	Pyrite	19.022	0.10	15.704	0.10	39.194	0.10	0.825	0.012	2.0605	0.018
SJ-I-B11-6	Pyrite	19.146	0.13	15.719	0.05	39.347	0.14	0.8210	0.118	2.0551	0.046
SJ-I-A9-10	Pyrite	18.962	0.02	15.682	0.01	39.075	0.02	0.8270	0.009	2.0607	0.014

Four sulphide samples were selected for Pb isotopic analysis to compare their Pb isotopic signatures with other samples from the area including sulphides from Klondike and White Gold gold-bearing orogenic veins, as well as igneous feldspars from Early and mid-Cretaceous and Late Cretaceous intrusions in the region. Samples SJ-R-A9-11, SJ-A-A9-10 and sample SJ-I-A9-

7 were taken from the silified zone in the central part of the mapping area (Plate 1) whereas sample SJ-I-B11-6 is a sample quartz-bioite schist from the southern part of the mapping area. Pyrite was separated from samples SJ-R-A9-11, SJ-I-B11-6 and SJ-A-A9-10 and arsenopyrite was separated from sample SJ-I-A9-7.

Unfortunately a usable analysis was not obtained from the arsenopyrite from sample SJ-I-A9-7; therefore, only three isotopic ratios are reported here. Figure 23 shows the distribution of the Pb isotopic signatures for the major intrusive phases and orogenic vein systems analysed from the western Yukon. The three pyrite analyses from the Black Hills Creek veins fall well

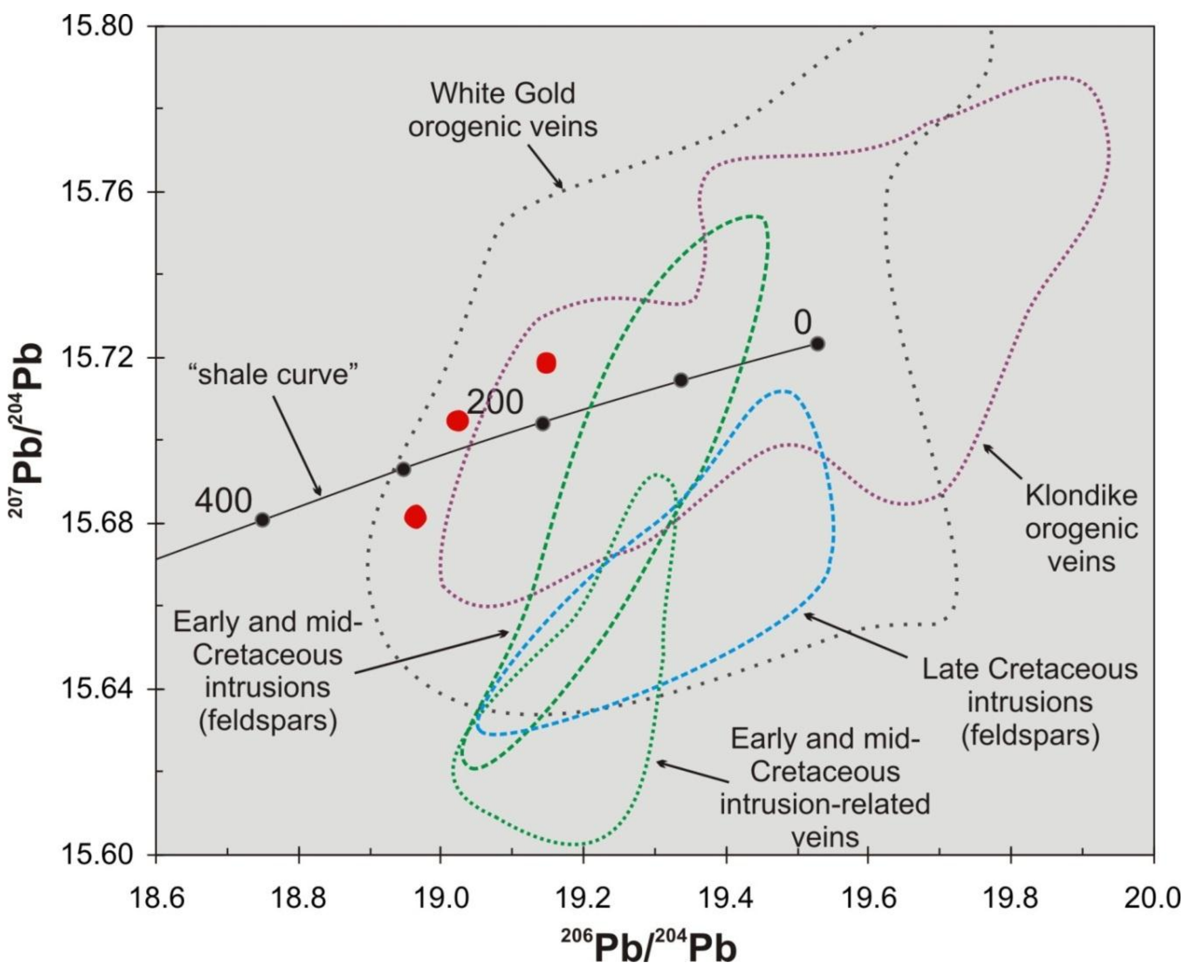

Figure 23: The Pb isotope plot demonstrates the different fields of Pb signatures from various Early to Late intrusions in the Yukon-Tanana terrane in western Yukon, as well as sulphides from gold-bearing orogenic veins in the Klondike and White Gold districts. The red dots are isotopic compositions from the three sulphide samples from the study area along Black Hills Creek.

outside of the fields for igneous Pbs from Early and Late Cretaceous intrusions in western Yukon (Fig. 23), indicating that the metals were not derived from any of these intrusions. The substantial amount of scatter shown by the three analyses from the Black Hills Creek area is more typical of what is observed from orogenic veins such as those in the Klondike and White Gold areas (Fig. 23). Hence the Pb isotopic data suggests the Black Hills Creek sulphide bearing veins are orogenic rather than intrusive related.

Chapter 5

5.1 Discussion

The Whiskey property lies to the west of the recently discovered White Gold deposit owned by Kinross and to the south of the historic Klondike goldfields. The structural model defined by MacKenzie *et al.* (2006, 2008 and 2010) has suggested that there are important stages of deformation in the Klondike and White Gold areas that are important to gold mineralization. The suggestion that D_4 structures could host mineralization has increased the emphasis exploration companies such as Smash Minerals place on the structural understanding of their property. This study attempted to constrain the structural evolution of the study area and to determine the timing of mineralization in the context of the aforementioned structural model.

The Black Hills Creek area that was mapped as part of this study was not observed to contain all five components of the structure model described in Table 1. Nevertheless, the area provided an opportunity to complete a detailed study of the lithological and structural relationships present.

From the mapping completed during the 2011 summer season three main lithologic units were identified including a quartz-biotite schist, a strongly deformed quartzite and a granitic dyke. The cross-cutting relationships established that the felsic dykes were emplaced following the deformation event that caused the pervasive foliation. The dykes are locally foliated, indicating that they may have been affected by the late stages of the compressive deformation affecting the host units. This type of variable foliation is consistent with that seen in Jim Creek pluton. The Jim Creek pluton is a massive to locally foliated garnet-quartz monzonite that is dated at 252.5 Ma (Allan *et al.,* 2011). There is also a strong geochemical correlation between the dykes and the Late Permian Jim Creek Pluton (Fig. 20).

Monazites and zircons from the granitic dykes did not readily support the field relationships observed. As the dykes cross-cut the pervasive foliation at a low angle, the dykes must be younger than the foliation and yet sample SJ-D-A8-13 yielded a concordant analysis with an age of 321.4 Ma and sample SJ-D-A6-17 bore three younger dates of 263 ± 1.7 Ma, 248.2 ± 0.8 Ma and 234.2 ± 1.0 Ma. The older monazite age of 321.4 Ma has been interpreted to represent the age of an older metamorphic core that was entrained and the dyke intruded. The younger monazite ages may record late monazite growth within the dyke that correlates to the long monazite growth period found in the schist (260-248Ma). A final concordant zircon analysis dates the dyke to be 257.3 ± 5.6 Ma (Fig. 22C) which emplaces the dyke after peak metamorphism at ~260 Ma supporting the field relationships observed.

Additional U-Pb dating of monazite from the biotite-schist gave concordant analyses with dates of 260.7 ± 1.1 Ma and 248.1 ± 0.8 Ma. These ages are interpreted to indicate the age of peak metamorphism (260.7 ± 1.1 Ma) which corresponds to the Klondike orogeny (Beranek and Mortensen, 2011). Furthermore, the range in ages (260 Ma -248 Ma) parallels the range of

Table 4: The structural evolution and interpreted ages of deformations events of the Black Hills Creek

Regional Deformation Event	Black Hills Creek Structures	Inferred age
D_3	Inclined tight-isoclinal folds, with fold axis parallel to pervasive foliations	**???** Post Felsic dyke emplacement
Felsic intrusions	Granitic dykes that locally contain weak fabric	Intruded before the end of D2 since parallel fabrics are observed in the dyke **257.3 ± 5.6 Ma**
D_1 and D_2	Pervasive foliation striking NW-SE, isoclinal folds	**260.7 ±1.1 Ma**

monazite growth observed in the Stewart River region (Berman *et al.* 2007) which suggests these rocks were buried deep for a over 12 Ma at sufficient depth for monazite to grow

Peak metamorphism, interpreted to be 260 m.y ago, is considered the main deformational event that produced the pervasive foliation observed in the study area (Table 4). The event, interpreted as $D_{2,}$ produced NW-SE striking foliation that generally shallowly dips (20°-40°) to the SE (Fig. 24A). This foliation was subsequently intruded by granitic dyke either in late D_2 or just after.

Tight to isoclinal folds observed in the study area fold the pre-existing, pervasive D_2 fabric. The majority of these structures are on a cm to m scale however in the northern section the exposure of the felsic volcanic unit is interpreted to represent two opposing limbs of a tight inclined fold. The fold axis appears to be striking NW-SE, parallel to the pervasive foliation indicating that the later folding event (D_3) folded the D_2 fabric along the same orientation. D_3 is interpreted to postdate the granitic intrusions since dykes are incorporated into the hinge of the D_3 felsic volcanic fold in the northern part of the study area. Figure 24 illustrates the structural evidence and the inferred timing of the deformational events. A highly silicified zone found in the central part of the study area trends NE-SW and can interpreted to be a late brittle feature because of its different orientation. Samples SJ-R-A9-11 and SJ-A-A9-10 were collected from this silicified zone and subjected to Pb-isotope analysis. The sulphides loosely correlate with the signatures of orogenic veins from elsewhere in the western Yukon.

The two generations of quartz veins (bluish-grey and white) appear to be associated with the emplacement of the granitic dykes. They are not limited to the dyke structures however they are commonly found both cross-cutting dykes and parallel to dyke contacts. These veins are therefore interpreted as being emplaced at the same time as the dykes. Neither of these types of veins contain applicable mineralization (Appendix 5).

A total of 14 samples were assayed however none recovered any promising gold values. Additional Ar-Ar dating should be done on the coarse grained muscovite that is commonly found along the margins of the quartz veins. This could yield a cooling age of hydrothermal mica related to vein formation, although the rocks are susceptible to younger, overprinting thermal events.

It is important to note that even though the Black Hills Creek area does not appear to contain D_4 or D_5 structures as defined by the model these structures are generally rare or larger features and may not be have been observable in the small mapping area.

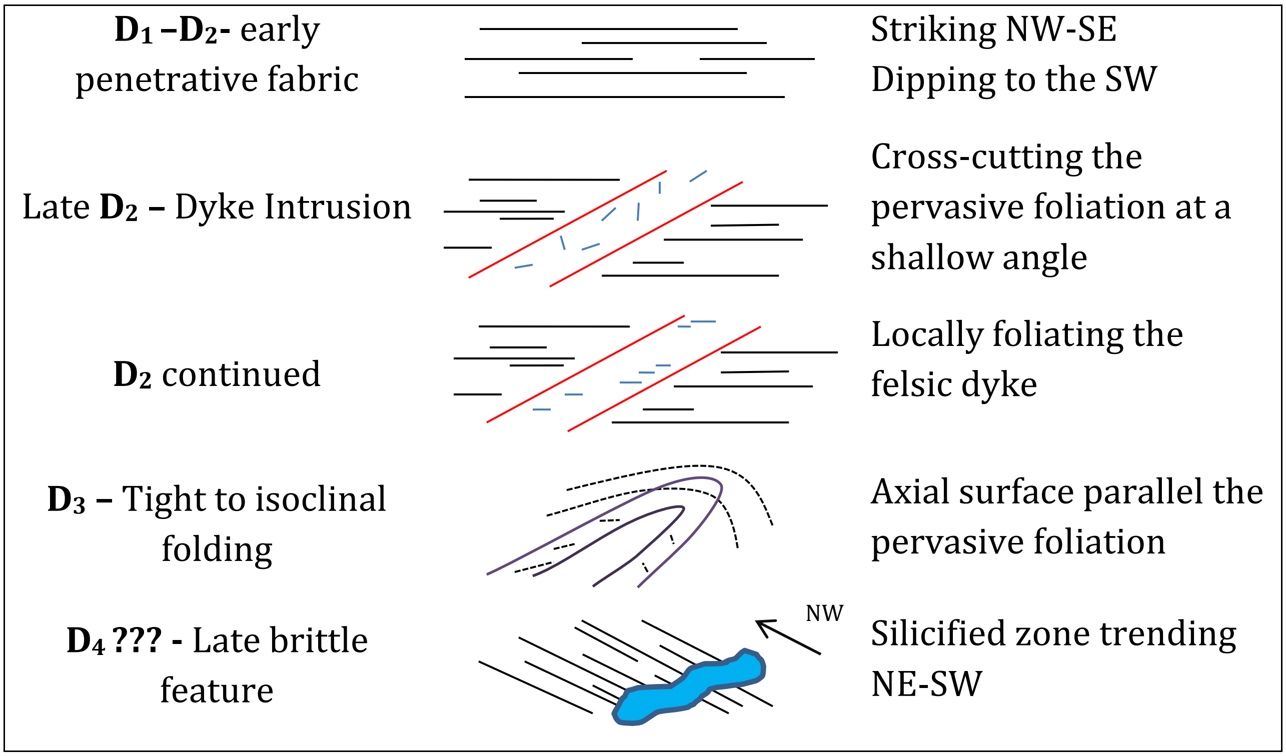

Figure 24: Interpretive sketches of the structural evolutions of the Black Hills Creek area

5.2 Conclusion

The study concluded that although all five phases of deformation anticipated from the model by MacKenzie *et al.* (2006, 2008 and 2010) are not present within the Black Hills Creek study area the structural evolution correlates with the regional development. With a peak metamorphic age of 260 m.y ago correlating to the Klondike orogeny and felsic dykes resembling both mineralogically and chemically the Permian intrusives of the area it can be said that rocks the Black Hills Creek have experienced at least two events (D_2 and plutonic intrusions) and one subsequent folding event of unconstrained age that parallel the region model defined by MacKenzie *et al.*, (2006, 2008 and 2010). Therefore the surrounding Smash Mineral claims could be expected to contain late brittle structures that are thought to host the mineralization in the neighbouring White Gold property. Although there was hydrothermal activity associated with Late Permian magmatism in the form of quartz veins, these have yet to know evidence of gold mineralization on the Whiskey property.

References

Allan, M., Mortensen, J.K., Hart, C., Bailey, L., McKenzie, G., Cox, D., Wrighton, T., Ciolkiewicz, W., and Chapman, R., (2011). Interim report and meeting notes, *Yukon Gold Project Technical Meeting #3* (pp. 6-13)

Beranek, L.P, and Mortensen, J.K. (2011). The timing and provenance record of the Late Permian Klondike orogeny in northwestern Canada and arc-continent collision along western North America. *Tectonics.* v.30, p. 1-23

Berman, R.R., Ryan, J.J., Gordey, S.P., and Villeneuve, M. (2007) Permian to Cretaceous polymetamorphic evolution of the Stewart River region, Yukon-Tanana terrane, Yukon, Canada: P-T evolution linked with *in situ* SHRIMP monazite geochronology. *Journal of Metamorphic Geology.,* v. 25, p. 803-827

Bostock, H.S., (1942). Ogilvie, Yukon Territory. Geological Survey of Canada, Map 71A (1:253 440-scale map with marginal notes).

Colpron, M., Nelson, J.L., and Murphy, D. C., (2006a). A tectonostratigraphic framework for the pericratonic terranes of the northern Coridllera. In: *Paleozoic Evolution and Metallogeny of Pericratonic Terranes at the Ancient Pacific Margin Paper 45* (eds Colpron, M., and Nelson, J.L.), pp. 1-23. Geological Association of Canada, St. Johns, Newfoundland

Cox, S., and Ruming, K. (2004). The St. Ives mesothermal gold sustem, Western Australia - a case of golden aftershocks? *Journal of Structural Geology, v. 26*, p. 1109-1125.

Gerstenberger, H. and Haase, G., (1997), A highly effective emitter substance for mass spectrometric Pb isotope ration determinations, *Chemical Geology,* v. 136, p.309-312

Global Business Reports. (2011). Yukon: An unexplored golden nugget. *Engineering and Minning Journal*, 65-71.

Gordey, S.P., and Ryan, J.J, (2005) Geology map, Stewart River area (115 N, 115-O and part of 115J), Yukon Territory, Geologic Survey of Canada, Open File 4970 (1 sheet, 1:250 00 scale)

Irvine, T.N., and Baragar, W.R.A., (1971), A guide to the chemical classification of the common volcanic rocks, *Canadian Journal of Earth Science,* v.8, p.523-548<

Le Bas, M.J., Le Maitre, R.W., Streckeisen, A., and Zanettin, B., (1986), A chemical classification of volcanic rocks based on the total alkali-silica diagram, *Journal of Petrology*, v.27, 9. 745-750

Mattinson, J.M., (2005), Zircon U-Pb chemical abrasion ("CA-TIMS") method: Combined annealing and multi-step partial dissolution analysis for improved precision and accuracy of zircon ages, *Chemical Geology,* v. 220,p.47-66

Mackenzie, D., & Craw, D. (2011). The structural setting of the Smash Minerals Claim Group in the Stewart River area, Yukon, Canada. University of Otago, Geology Department. Dunedin: Smash Mineral Corporation.

MacKenzie, D., & Craw, D. (2012). Contrasting structural setting of mafic and ultramafic rocks in the Yukon-Tanana Terrane. *Yukon Exploration and Geology*.

MacKenzie, D., Craw, D., & Mortensen, J. (2008). Structural controls on orogenic gold mineralisation in the Klondike goldfield, Canada. *Miner Deposita, 43*, 435-448.

MacKenzie, D., Craw, D., Mortensen, J., & Liverton, T. (2006). Structure of schist int he vicinity of the Klondike goldfield, Yukon. *Yukon Exploration and Geology*, 189-212.

Mortensen, J. K. (1990). Geology and U-Pb geochronlogy of the Klondike District, west central Yukon Territory; *Canadian Journal of Earth Science,* v.27, p. 903-914

Mortensen, J.K. (1996), Geological maps of the northern Stewart River map area, western Yukon (6 sheets; 1:50 000 scale, with marginal notes): Canada/Yukon Geoscience Office, Open File 1996-1

Mundil, R., Ludwig, K.R., Metcalfe, I. and Renne, P.R., (2004) Age and timing of the Permian mass extinction: U/Pb dating of closed system zircons, *Science*, v.305, p.1760-1763

Mortensen, J.K. and Hart, C.J.R., (2010), Late and post-accretionary Mesozoic magmatism and metallogeny in the northern Cordillera, Yukon and east-central Alaska, *Geological Society of America,* Abstracts with Program, v.42, p.676

Nelson, J., & Colpron, M. (2007). Tectonics and metallogeny of the Bristish Columbia, Yukon and Alaskan Cordillera, 1.8 Ga to the Present. In G. W.D, *Minerals Deposits of Canada: A synthesis of Major Deposits-Types, District metallogeny, the evolution of Geological Provinces and Exploration Methods* (pp. 755-791). Ottawa: Geological Association of Canada, Mineral Deposits Division

Pearce, J.A., Harris, N.B.W., and Tindle, A.C., (1984), Trace element discrimination diagrams for the tectonic interpretation of granitic rocks, *Journal of Petrology,* v. 25, p.956-983

Piercey, S.J. and Colpron, M., (2009), Composition and provenance of the Snowcap assemblage, basement to the Yukon-Tanana, northern Cordillera: Implications for Cordilleran crustal growth, *Geosphere,* v.5, p.439-464

Scates, J.S., and Friedman, R.M., (2008), Precise age of the platiniferous Merensky Reef, Bushveld Complex, South Africa, by the U-Pb zircon chemical abrasion ID-TIMS technique, *Society of Economic Geologist,* v.103, p.465-471

Shaud, S.J., (1943), *The Eruptive Rocks,* 2nd edn. New York: John Wiley, p. 444

Thirlwall, M.F. (2000), Multicollector ICP-MS analysis of Pb isotopes using a ^{207}Pb-^{204}Pb double spike demonstrates up to 400 ppm/amu systematic errors in Tl-normalization, *Chemical Geology,* v.184, p. 255-279

Winchester, J.A., and Floyd, P.A., (1977) Geochemical discrimination of different magma series and their differentiation products using immobile elements, *Chemical Geology,* v.20, p. 325-343

Appendix 1 - List of Yukon Gold Project Consortium

Aldrin Resource Corp.

Barrick

Full Metal Minerals

Gold Fields

Kinross

Northern Freegold Resources Ltd.

Radius Gold Inc.

Silver Quest Resources Ltd.

Taku Gold Corp.

Teck

Underworld Resources

Canada Geological survey

Appendix 2 – Geochemical Sample Photos


R-A8-16
3 cm


R-B3-19
1.5 cm

Appendix 3 - Geochemical Results

SAMPLE	Ag_ppm	Ba_ppm	Ce_ppm	Co_ppm	Cr_ppm	Cs_ppm	Cu_ppm	Dy_ppm
SJ-D-A6-17	<1	737	26.3	<0.5	10	1.89	<5	7.51
SJ-D-A8-13	<1	2590	58.2	0.9	10	2.25	5	2.04
SJ-D-A8-16	<1	569	28.1	0.8	10	1.17	<5	1.71
SJ-D-B3-19	<1	>10000	62.9	0.8	10	0.74	14	5.59
IND11-05_117.0m	<1	7250	322	1.7	10	3.91	7	8.2

Er_ppm	Eu_ppm	Ga_ppm	Gd_ppm	Hf_ppm	Ho_ppm	La_ppm	Lu_ppm	Mo_ppm	Nb_ppm
6.41	0.32	24.3	3.28	1.7	1.81	13.7	1.41	<2	4.1
1.1	1.38	13.9	2.77	4.3	0.38	30.6	0.19	2	5.7
1.04	0.62	15.3	1.79	2.2	0.35	15.9	0.16	<2	8.6
3.13	1.2	13.1	6.23	5.6	1.07	34.7	0.44	<2	10.4
5.98	2.72	16.2	10.05	6.1	1.87	180	0.98	<2	6.3

Nd_ppm	Ni_ppm	Pb_ppm	Pr_ppm	Rb_ppm	Sm_ppm	Sn_ppm	Sr_ppm	Ta_ppm	Tb_ppm
10.8	<5	15	3	135	2.97	2	30.8	1.1	0.9
22.6	<5	42	6.33	165.5	4.17	1	155.5	0.4	0.39
10.7	<5	19	3	70.2	2.13	1	105	1.3	0.29
28.5	<5	14	7.38	215	6.53	2	503	0.9	1.03
114	<5	33	34.2	109.5	15.05	1	561	0.2	1.36

SAMPLE	Th_ppm	Tl_ppm	Tm_ppm	U_ppm	V_ppm	W_ppm	Y_ppm	Yb_ppm
SJ-D-A6-17	8.39	<0.5	1.3	1.91	<5	<1	54.9	8.82
SJ-D-A8-13	16.4	0.5	0.19	2.68	6	<1	10.9	1.15
SJ-D-A8-16	5.08	<0.5	0.18	2.13	23	<1	11.3	1.05
SJ-D-B3-19	9.58	0.7	0.49	2.17	<5	1	32.3	2.76
IND11-05_117.0m	33.1	0.5	0.94	2.64	7	1	47.1	6.55

Zn_ppm	Zr_ppm	SiO2%	Al2O3%	Fe2O3%	CaO%	MgO%	Na2O%	K2O%	Cr2O3%
19	23	74.6	14.2	1.97	0.52	0.16	1.01	3.49	<0.01
35	142	74.9	14.2	1.05	0.81	0.29	1.95	5.32	<0.01
17	41	78.4	12.35	0.85	0.95	0.2	1.65	2.18	<0.01
22	195	76	10.1	0.29	0.24	0.02	1.49	5.71	<0.01
60	287	75.8	12.45	2.27	1.87	0.16	1.72	4.33	<0.01

TiO2%	MnO%	P2O5%	SrO%	BaO%	LOI%	FeO%	Total%
0.02	0.44	0.08	<0.01	0.08	1.71	1.46	98.28
0.12	0.02	0.06	0.02	0.3	1.3	0.77	100.34
0.08	0.04	<0.01	0.01	0.06	1.79	0.38	98.56
0.17	<0.01	0.02	0.06	4.81	0.47	0.19	99.38
0.18	0.07	0.05	0.06	0.86	1	1.79	100.82

Ag_ppm	As_ppm	Cd_ppm	Co_ppm	Cu_ppm	Mov	Ni_ppm	Pb_ppm	Zn_ppm
<0.5	<5	<0.5	<1	<1	<1	<1	19	19
<0.5	6	<0.5	<1	3	<1	<1	45	28
<0.5	<5	<0.5	<1	2	<1	2	17	16
<0.5	<5	<0.5	<1	3	<1	<1	15	5
<0.5	<5	<0.5	<1	4	1	1	24	65

Appendix 4 – Sample Locations

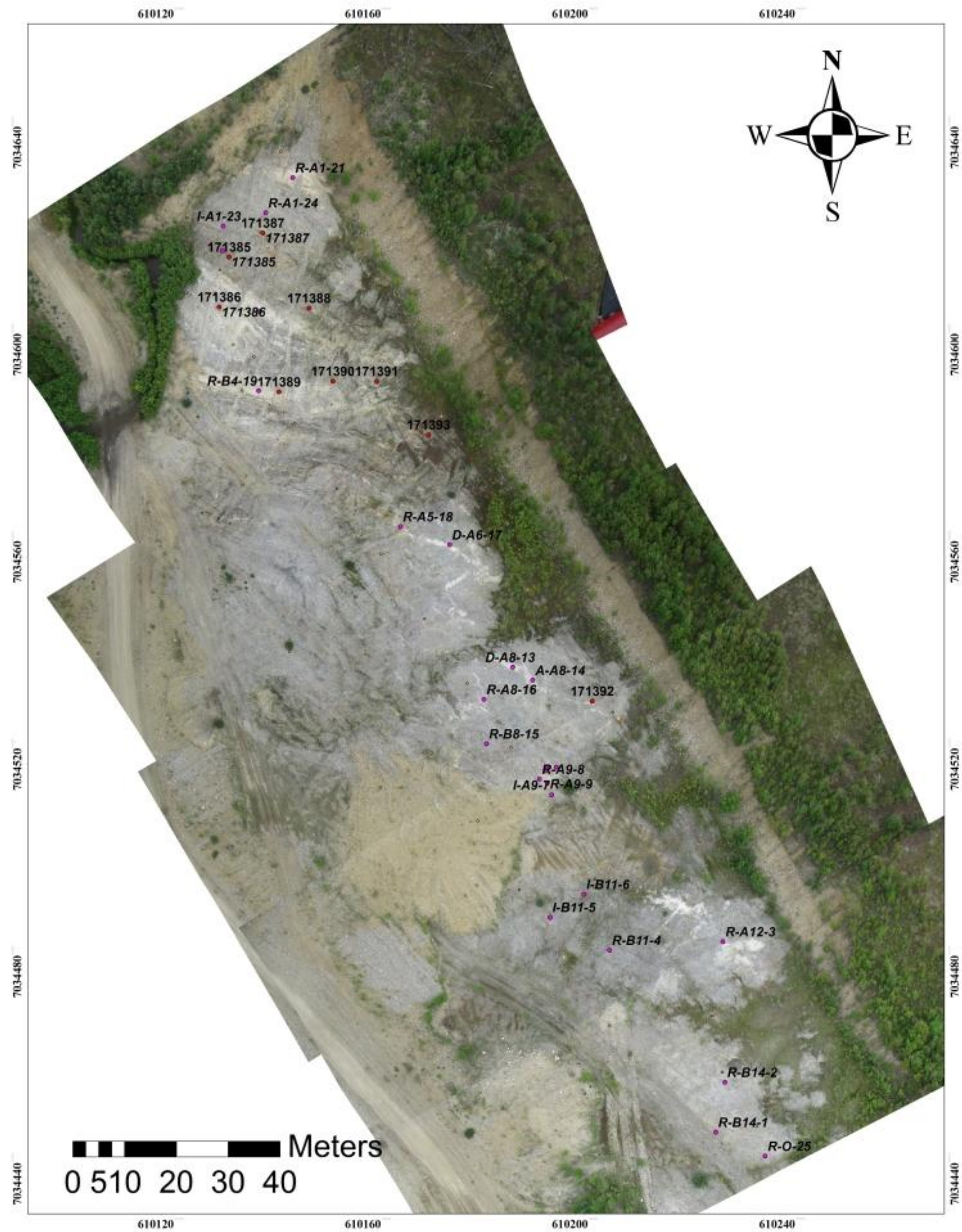

Appendix 5 – Assay Results

Sample	X-Coordinate	Y-Coordinate	Au_PPM	AU_PPB	AG_PPM	AL_PCT	AS_PPM
SJ-A-A8-14	610191.8221	7034546.275	0.002	2	0.05	0.12	1
SJ-I-A9-11	610194.2871	7034518.851	0.011	11	0.27	0.71	5.7
SJ-I-A9-10	610194.4332	7034519.487	0.002	2	0.28	0.96	3.5
SJ-I-B11-6	610201.709	7034494.966	0.003	3	0.39	0.48	16.7
47669			0.0025	2.5		0.17	0.5
171385	610133.1682	7034617.955	0.0025	2.5	0.22	1.24	2
171386	610131.2561	7034608.294	0.007	7	0.02	0.16	0.5
171392	610203.3197	7034532.231	0.012	12	0.35	0.96	81
171393	610171.6816	7034583.629	0	0	0.29	1.01	10
171389	610142.7998	7034591.905	0.0025	2.5	0.2	0.41	3
171390	610153.1991	7034593.959	0.006	6	0.11	1.08	3
171391	610161.6661	7034593.97	0.008	8	0.005	0.28	-1
171388	610148.5879	7034608.087	0.0025	2.5	0.4	1.1	2
171387	610139.685	7034622.58	0.0025	2.5	0.04	0.6	2

B_PPM	BA_PPM	BE_PPM	BI_PPM	CA_PCT	CD_PPM	CE_PPM	CO_PPM
<10	40	0.08	0.02	0.04	0.03	5.92	0.5
10	100	0.2	0.11	0.1	0.18	30.2	5.9
10	150	0.26	0.16	0.15	0.09	39.8	6.1
10	80	0.24	0.15	0.12	0.44	35.3	3.5
40	48	0.05	0.04	0.05	0.01	4.83	0.6
40	251	0.2	0.15	0.15	0.03	32.2	3.6
40	36	0.05	0.01	0.03	0.005	6.88	0.7
40	171	0.3	0.16	0.13	0.12	54	2.7
40	257	0.4	0.2	0.19	0.03	3.1	1.9
70	2810	0.5	0.06	0.25	0.04	44.8	0.7
70	138	0.3	0.06	0.29	0.14	29.6	6.3
70	87	0.1	-0.02	-0.01	-0.01	16.2	1.1
80	7520	0.1	0.38	0.47	0.02	24.2	2.9
60	96	0.3	0.09	0.07	0.02	17.3	1.5

CR_PPM	CS_PPM	CU_PPM	FE_PCT	GA_PPM	GE_PPM	HF_PPM	HG_PPM
20	0.15	9	0.27	0.37	<0.05	0.02	<0.01
30	0.6	33.9	1.82	3.31	0.09	0.06	0.03
42	1.16	30.1	2.19	4.34	0.1	0.1	0.01
17	1.36	21.7	1.89	2.24	0.09	0.09	0.4
7	0.6	1.5	0.21	0.5	0.05	0.025	0.005
58	3.6	16.1	2.55	7.2	-0.1	0.12	0.005
16	0.7	2.5	0.33	0.5	-0.1	0.025	0.005
167	2.11	20.3	1.63	4.1	-0.1	0.2	0.54
203	2.25	16	1.57	3.8	-0.1	0.16	0.09
128	0.29	7.7	0.35	2.5	-0.1	0.1	0.03
166	1.5	18.7	1.93	2.9	-0.1	0.15	0.03
157	0.42	2.5	0.52	1.7	-0.1	0.1	-0.01
137	1.11	48.5	1.87	4.6	-0.1	0.14	-0.01
127	0.71	5.7	0.91	2.6	-0.1	0.2	0.03

IN_PPM	K_PCT	LA_PPM	LI_PPM	MG_PCT	MN_PPM	MO_PPM	NA_PCT	NB_PPM
<0.005	0.05	3	0.7	0.02	35	0.17	0.02	0.08
0.014	0.14	15.4	5.6	0.33	121	1.29	0.02	0.18
0.021	0.29	20.1	7.2	0.48	203	0.76	0.02	0.45
0.011	0.21	19.5	3.7	0.13	68	1.59	0.01	0.32
0.01	0.13	2.6	0.04	0.02	104	0.95	0.03	0.08
0.02	0.72	17.2	0.08	0.67	222	2.05	0.03	1.29
0.01	0.07	3.4	0.01	0.04	36	1.38	0.01	0.42
-0.02	0.42	30.5	6	0.36	107	2.95	0.02	0.52
-0.02	0.41	14.3	11	0.32	115	2.48	0.01	0.46
0.03	0.23	22.5	2	0.04	43	0.76	0.03	1.33
-0.02	0.36	13.9	11	0.38	246	1.76	0.02	0.95
-0.02	0.22	2.8	1	0.12	69	1.37	0.05	0.49
0.03	0.55	13.6	7	0.5	339	0.8	0.09	1.12
-0.02	0.26	7.6	4	0.3	175	1.93	0.05	0.33

NI_PPM	P_PPM	PB_PPM	RB_PPM	S_PCT	SB_PPM	SC_PPM	SE_PPM	SN_PPM
1.6	120	20.7	2.6	0.01	<0.05	0.5	<0.2	<0.2
14.8	410	16.8	9.4	0.39	0.16	2.6	1.4	0.5
14.4	510	24.1	17.5	0.43	0.11	3.9	1.8	0.6
11.7	510	11.1	17.4	0.32	1.23	1.2	1.5	0.2
1.7	210	4.3	3.7	0.005	0.05	0.5	0.5	0.15
10.5	680	2.8	44.9	0.23	0.025	5.7	1	0.5
2.7	80	0.5	5.6	0.005	0.025	0.3	0.5	0.15
11.5	480	12.9	28.7	0.12	1.13	1.6	2	0.4
8.8	720	7.7	30.7	0.24	0.85	2	-1	0.4
3.5	1170	5.6	9.3	0.01	-0.05	2.3	-1	0.6
12.4	490	7.3	28.8	0.08	0.1	2.1	-1	-0.3
4.1	-50	1.8	15.3	-0.01	-0.05	1	-1	0.5
3.2	670	2.7	28.7	0.18	0.06	7.3	-1	0.9
4.2	210	6.7	12.2	-0.01	-0.05	1.1	-1	-0.3

SR_PPM	TA_PPM	TE_PPM	TH_PPM	TI_PCT	TL_PPM	U_PPM	V_PPM
1.6	<0.01	<0.01	0.8	<0.005	<0.02	0.5	2
6.6	<0.01	0.02	4.8	0.016	0.08	1.81	28
19	0.01	0.02	7.8	0.065	0.12	2.6	50
26	<0.01	0.04	6	0.02	0.19	2.06	23
2.7	0.025	0.025	1.6	0.005	0.01	0.29	1
6.7	0.025	0.08	7.7	0.16	0.24	1.06	93
1.8	0.025	0.025	0.6	0.005	0.03	0.17	4
33.9	-0.05	0.08	8	0.05	0.61	2.91	31
7	-0.05	0.05	6	0.05	0.28	1.42	35
30.5	-0.05	-0.05	8.6	0.01	0.06	1.26	3
16.8	-0.05	-0.05	9.2	0.11	0.2	1.35	35
2.6	-0.05	-0.05	7.2	0.02	0.08	0.48	4
40.9	-0.05	-0.05	3	0.23	0.2	0.51	42
4.7	-0.05	-0.05	6.3	-0.01	0.07	0.07	6

W_PPM	Y_PPM	ZN_PPM	ZR_PPM
<0.05	1.34	7	0.5
0.21	8.85	45	2.5
0.09	10.4	49	3.5
0.06	6.48	42	3.7
0.05	2.08	2	0.8
0.05	7.4	45	4.7
0.05	1.33	4	1.1
-0.1	8.52	37	7.5
-0.1	9.56	21	6.3
-0.1	14.8	7	2.5
-0.1	8.3	46	5.5
-0.1	0.96	7	3.1
0.8	11	30	3.5
-0.1	8.76	17	4.3